Institute of Earth- and Environmental Sciences
University of Potsdam

ALFRED-WEGENER-INSTITUT
HELMHOLTZ-ZENTRUM FÜR POLAR- UND MEERESFORSCHUNG

Mobilization of organic carbon and nitrogen in a retrogressive thaw slump on Herschel Island, Yukon Territory, Western Canadian Arctic

Master thesis

to attain the academic degree

Master of Science in Geoscience

Submitted by

Saskia Ruttor

Potsdam, 14.12.2015

1st Supervisor: **Prof. Dr. Hugues Lantuit**
University of Potsdam
Institut for Earth- and Environmental Science
Karl-Liebknecht-Str. 24-25, 14476 Potsdam-Golm

2nd Supervisor: **Dr. Michael Fritz**
Alfred-Wegener-Institute
Helmholtz Centre for Polar and Marine Research
Telegraphenberg A43, 14473 Potsdam

Contents

List of Figures

List of Tables

List of Abbreviations

°C	degree Celsius
µm	micormeter
DEM	digital elevation model
e.g.	Latin: exempli gratia; for example
Fig.	figure
Gt	gigaton
i.a.	Latin: inter alia; among others
IR	infra-red
km^2	square kilometer
m	meter
ml	milliliter
*mm*3	cubic millimeter
NDVI	normalized difference vegetation index
OM	organic matter
RTS	retrogressive thaw slump
TC	total carbon
TN	total nitrogen
TOC	total organic carbon
VPDB	Vienna Pee Dee Belemnite

Abstract

Herschel Island, located in the southern Beaufort Sea, Western Canadian Arctic, shows a clear response to the global warming. Due to its ice-rich permafrost it is highly affected by environmental forcing and known for its high erosion rates and retrogressive thaw slump activity. Even though retrogressive thaw slumps have an effect on carbon and nitrogen cycling, until now there is not much known about the processes and carbon and nitrogen availability within a retrogressive thaw slump at a circumarctic scale. To provide new insides in this particular field, the retrogressive thaw slump "Slump D" on Herschel Island was divided into undisturbed (tundra zone, permafrost zone), and disturbed zones (mud pool zone, slump floor zone) and sampled via a fishnet grid. The tundra, mud pool and slump floor zones were sampled at 0 to 30 cm depth, for the permafrost zone permafrost profiles of up to 340 cm depth were sampled. In total 100 samples were analysed in their biogeochemical parameters (total organic carbon(TOC)-, total carbon(TC)-, total nitrogen(TN)-content) and stable isotope content ($\delta^{13}C_{org}$). The organic carbon source was determined for all zones to illustrate eventual differences in the deposition milieu. To show the degree of decomposition and degradation during the slumping process TOC/TN-ratio and $\delta^{13}C_{org}$ were used as proxys. The results show that the tundra zone has the highest TC-, TOC- and TN-values follwed by the permafrost zone. The lowest values are determined for the slump floor and the mud pool zone. All of the zones show similar $\delta^{13}C_{org}$-values of -26.9 ‰ but obvious differences in the TOC/TN-ratio. From the results it is concluded that the tundra zone shows a higher degradation than the permafrost zone but less than the mud pool and slump floor zone. Based on the high TOC/TN-values for the permafrost zone a vulnerable zone where carbon and nitrogen is available for decomposition during thawing processes is indicated. Due to the better quality of the organic matter within the permafrost zone labile carbon can be released right after thawing. The mud pool as well as the slump floor are highly degraded and store the more stable carbon which stays in the soil for several years. Within the slump floor zone no differences in degradation or composition are visible even though there is a mixture of old and new vegetated areas. With this findings the first step is made to understand the influence of degrading permafrost on carbon and nitrogen dynamics within a retrogressive thaw slump.

Zusammenfassung

Herschel Island, im Süden der Beaufort See, im Westen der kanadischen Arktis gelegen, reagiert deutlich auf die Klimaerwärmung. Wegen des eisreichen Permafrosts ist die Insel besonders anfällig gegenüber Naturkräften und bekannt für hohe Erosionsraten und aktive Retrogressive Thaw Slumps. Obwohl Retrogressive Thaw Slumps sowohl den Kohlenstoff- als auch den Stickstoffkreislauf beeinflussen, sind die Prozesse und die Verfügbarkeit von Kohlen- und Stickstoff eines Retrogressiven Thaw Slumps auf zirkumarktischer Basis bis heute noch nicht komplett erforscht. Um neue Einblicke diesbezüglich zu bieten, wurde der Retrogressive Thaw Slump "Slump D" auf Herschel Island in ungestörte (Tundra Zone, Permafrost Zone) und gestörte Zonen (Mud Pool Zone und Slump Floor Zone) unterteilt und nach einem netzartigen Schema beprobt. Proben für die Tundra, Mud Pool und Slump Floor Zonen wurden in Tiefen von 0 bis 30 cm entnommen, Permafrost-Profile reichen bis in eine Tiefe von 340 cm und repräsentieren die Permafrost Zone. Insgesamt wurden 100 Proben auf ihre biogeochemischen Parameter (gesamter organischer Kohlenstoff (TOC), Gesamtkohlenstoff (TC), Gesamtstickstoff (TN)) und auf stabile Isotope ($\delta^{13}C_{org}$) analysiert. Die Herkunft des organischen Kohlenstoffs wurde für alle Zonen bestimmt, um mögliche Unterschiede in den Ablagerungsmilieus zu erkennen. Das TOC/TN-Verhältnis und $\delta^{13}C_{org}$ wurden als Proxys für den Grad an Zersetzung und Degradation während des Rutschungs- und Tauprozesses verwendet. Die Ergebnisse zeigen, dass die Tundra Zone die höchsten TC-, TOC- und TN-Werte aufweist, gefolgt von der Permafrost Zone. Die niedrigsten Werte sind für die Slump Floor und die Mud Pool Zone gemessen worden. Alle Zonen zeigen ähnliche $\delta^{13}C_{org}$-Werte von -26.9 ‰, aber auffällige Unterschiede in den TOC/TN-Verhältnissen. Anhand der Ergebnisse kann gesagt werden, dass die Tundra Zone einen höheren Grad an Degradation als die Permafrost Zone aufzeigt, jedoch einen niedrigeren Grad verglichen zu der Mud Pool und der Slump Floor Zone. Das hohe TOC/TN-Verhältnis der Permafrost Zone steht für eine hohe Empfindlichkeit gegenüber der Mobilisierung von Kohlenstoff und Stickstoff während des Tauprozesses. Der labile Kohlenstoff wird, bedingt durch die gute Qualität des organischen Materials in der Permafrost Zone, während des Tauprozesses freigesetzt. Sowohl die Mud Pool als auch die Slump Floor Zonen zeigen einen hohen Grad an Degradation, und speichern hauptsächlich den stabileren Kohlenstoff, welcher den Boden für mehrere Jahre nicht verlässt. Die Slump Floor Zone an sich weist keine unterschiedlichen Degradations- und Zersetzungsgrade auf, obwohl länger bewachsene und erst kürzlich bewachsene Flächen unterschieden werden können. Diese Arbeit trägt dazu bei, die Einflüsse des degradierenden Permafrosts auf die Kohlenstoff- und Stickstoffverteilung in einem Retrogressiven Thaw Slump zu verstehen.

1 Introduction

1.1 State of the Art

Vast amounts of carbon are stored in permafrost which is covering approximately 24 % of the northern hemisphere's landmass and is present along 34 % of the Earth's coast (French, 2007; Lantuit et al., 2012a). About 40-60 Gt nitrogen and 1700 Gt of organic carbon are stored within permafrost (Weintraub and Schimel, 2003; Tarnocai et al., 2009; Harden et al., 2012; Hugelius et al., 2014; Schuur et al., 2013, 2015). This is more than four times as much organic carbon than all organic carbon emitted from fossil fuel combustion (350 Gt) since 1850 (Sundquist and Visser, 2004; Hilton et al., 2015). In the northern circumpolar regions the uppermost three meters of permafrost contain 1035 ± 150 Gt of carbon (Hugelius et al., 2014).

Since the beginning of the 19th century annual air temperatures have been increasing. In 1980, temperatures have been twice as high in the Arctic compared to the rest of the world. According to the report of Pachauri et al. (2014) average air temperature increases between 1°C (RCP2.6) and 8°C (RCP8.5) are expected by the end of the 21st century. This may result in increasing sea surface temperatures, decreasing sea ice coverage, melting ice caps and glaciers, sea level rise, higher coastal erosion rates (Pachauri et al., 2014), and most important in thawing permafrost (Romanovsky et al., 2010), causing release of greenhouse gases into the atmosphere and transfer of organic matter into aquatic environments (Schädel et al., 2014). Carbon in surface permafrost is, and will be, the most vulnerable pool during this century given the retreat of permafrost to deeper layers (Zimov et al., 2006). Within this century it is likely that almost all near-surface permafrost will disappear (Lawrence and Slater, 2005). With a warming climate and a thawing permafrost erosion rates will increase most notably for the Arctic coasts, because of the high ice content and the mostly unlithified texture of these coasts (Serreze and Francis, 2006; Lantuit and Schirrmeister, 2012b). Eroding permafrost coasts can be a thread to industry and community infrastructure, as it can result in land loss

(U.S., 2003; Forbes et al., 2011; Lantuit and Schirrmeister, 2012b). With a disbalance of the thermal equilibrium, resulting in thawing permafrost and warming climate, thermokarst occurs. Thermokarst plays an exceptional role, as it leads to massive release of sediments and organic carbon that is stored within the coast (De Krom, 1990; Kokelj et al., 2013). One of the most spectacular forms of thermokarst are retrogressive thaw slumps (RTS). Coastal erosion is amplified where RTS occur and is diminished where they are absent (Lantuit and Pollard, 2008).

Active RTSs move inland rapidly, which is a serious problem for the coastal infrastructure (Lantuit and Pollard, 2005) and includes the removal of surface vegetation during ground collapse. The activity and stability of RTSs are very sensitive to environmental forcing (Kokelj et al., 2015). With higher erosion rates RTS could play a significant role in the carbon cycle (Tarnocai et al., 2009; Kokelj and Jorgenson, 2013). By increasing frequency and magnitude of RTS and further degrading permafrost, terrestrial organic carbon in form of dissolved organic carbon (DOC, <0.45μm) and particular organic carbon (POC, >0.45μm), summed up as total organic carbon (TOC), gets mobilized by microbes. This makes carbon as well as nitrogen assessable for the carbon and nitrogen cycle, for degradation and decomposition (Guo and Macdonald, 2006; Strauss et al., 2015). Hence permafrost as a long term carbon and nitrogen storage turns due to the climate change into a carbon and nitrogen source (Schuur et al., 2009, 2015).

Concerning the size of the organic carbon pools and the vulnerability to climate forcing at high latitudes, carbon stored in permafrost and the processes during permafrost degradation are not yet fully understood (Schuur et al., 2008). Even though RTSs could contribute to alter the carbon and nitrogen budget, they are not yet included in the carbon budget and Earth system models used to predict the effects of climate change (Kokelj and Jorgenson, 2013; Schuur et al., 2013; Koven et al., 2015). It is important that all carbon pools are recognised in future climate models and that processes controlling the carbon balance are understood (Canadell et al., 2007). How much DOC gets released is already known for some regions of Canada (Douglas et al., 2011; Fritz et al., 2011; Tanski, 2013; Larouche et al., 2015) but how carbon and nitrogen affect the nearshore ecosystem has not been studied in much detail. How much POC gets transported from coastal cliffs is known by now (Couture, 2010), but it is not known how much POC gets transported to the ocean by RTSs on a circumarctic scale.

Instead of POC this study will refer to TOC, because of sample treatment, here not all of the water within the soil samples was removed before freeze-drying. This study helps to get an idea of how much TC, TOC and TN is stored in a RTS, to what extent it has been degraded and thus how much TOC could be transported to the near shore zone and potentially affect marine ecosystems. By measuring $\delta^{13}C_{org}$-values and the elemental TOC/TN-ratio, the organic carbon source was determined to understand differences within the slump system. $\delta^{13}C_{org}$-values and the elemental TOC/TN-ratio were further used as a proxy of decomposition and degradation. An increasing degradation of TC, TOC and TN during the slumping process of the RTS is hypothesised.

1.2 Aims and Objectives

This study will contribute to a better understanding of carbon dynamics within a retrogressive thaw slump. The aim is to reveal differences in total organic carbon (TOC), total carbon (TC) and total nitrogen (TN) between undisturbed (tundra zone, permafrost zone) and disturbed zones (mud pool zone, slump floor zone) within a RTS. By determining the concentration of TOC and TN, the potential of how much carbon and nitrogen could be transported to the near shore zone and how much carbon and nitrogen could potentially be released as greenhouse gases can be valuated. The specific objectives of this thesis are to

1. Quantify TC, TOC and TN concentrations in a RTS system;
2. Identify the origin of organic material in a RTS system regarding $\delta^{13}C_{org}$ and the elemental TOC/TN-ratio;
3. Estimate the degradation and decomposition within the slumping process of a RTS system.

2 Background

2.1 Periglacial Environments

The term “periglacial” was first used by the polish geologist Von Lozinski (1909) to describe climate and morphology of the Carpathian Mountains in central Romania. Nowadays it is used for cold-region, non—glaciated landscapes and not necessarily referring to the proximity of glaciers and ice sheets or its age, as the name would suggest (French, 2007). The periglacial environment is characterised by the presence of perennially frozen ground and intense frost action processes (Heginbottom et al., 2012). In the Arctic, this environment is associated with a limited annual input of sunlight compared to other regions on Earth. The angle of incident radiance is lower during the summer months (Woo and Ohmura, 1997). Further, periglacial environments are characterized by a relatively high snow cover, which reflects the incoming radiation and thus shows a high albedo effect. Freeze and thaw processes are unique for periglacial landscapes and can lead to special morphologic features like ice wedges, polygonal nets, palsas, rock glaciers, frost mounds, thermokarst depressions and lakes (French, 2007).

2.2 Permafrost

Permafrost is defined as perennially-frozen ground with a temperature of 0°C or below for at least two consecutive years (Van Everdingen, 2005). The term “frozen” has to be used carefully because permafrost ground can also be not frozen ground with a temperature below 0 °C, due to the surrounding sediment, depressing the freezing point of pore water below 0°C. For that reason permafrost is not defined by the moisture content or the state of water but by the temperature of the ground material. Alternatively, permafrost could also be defined as perennially cryotic ground (Harris et al., 1988; French, 2007). Fig. 2.1 shows a typical temperature profile of permafrost affected ground. With increasing depth the temperature

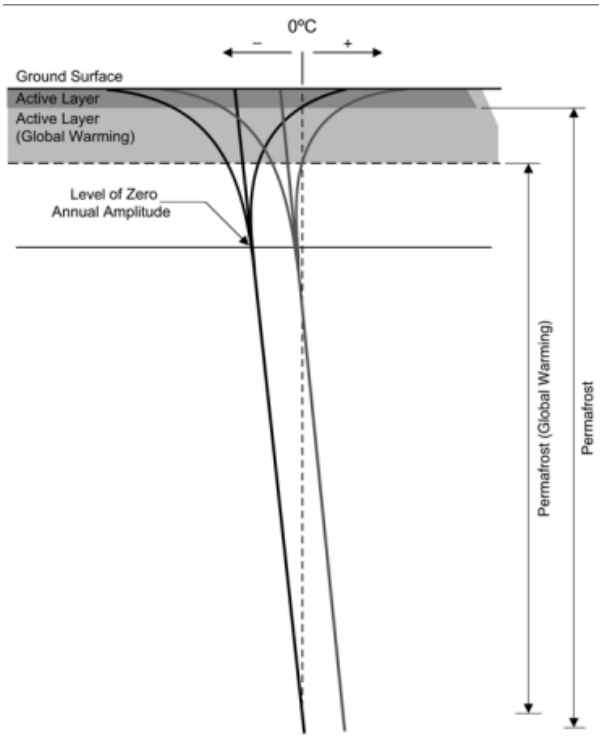

Figure 2.1: Permafrost temperature profile from the ground surface to the base of the permafrost at 0°C. 0°C represented as a dashed line, to the right increasing temperatures and to the left decreasing temperatures, black curve shows current conditions, grey curve shows condition including climate warming (according to U.S., 2003).

decreases due to the geothermal gradient.

A typical feature of permafrost affected sediments and soils is the active layer (Fig. 2.1). This layer describes the upper part of the sediment, which seasonally thaws and refreezes (Burn and Zhang, 2009). The active layer depth varies from less than 0.5 meters in areas with vegetation cover, to several meters in areas of exposed bedrock (Smith et al., 2001). Its thickness depends on local factors like climate, snow cover and vegetation, the presence of an organic layer, and moisture conditions (Wolfe et al., 2000; Smith et al., 2001; Smith and Burgess, 2004; French, 2007). Roots cannot penetrate permafrost so the vegetation cover is only present in the active layer (Margesin, 2009). The thickness of the active layer influences plant rooting, hydrological processes and most importantly the quantity of soil organic matter exposed in the high latitudes mainly during the summer month (Schuur et al., 2008). With a deepening of the active layer, the ground can lose its stability and can be subject to degradation. The freezing and thawing of the active layer mixes different soil layers, a phenomenon called cryoturbation. The thickness of permafrost can vary from around 1 m to more than 1500 m depending on

the regional climate, topographic, sediment composition, moisture conditions, and vegetation (Schuur et al., 2008). With higher latitudes permafrost thickness increases, because of the decreasing temperature (Schuur et al., 2008). Within the permafrost, especially in peatlands and sedimentation environments deposited during the Pleistocene, accumulation and incorporation of organic matter (OM) is high (Zimov et al., 2006; Strauss et al., 2013). Accumulation and distribution of carbon in permafrost soils depends on several features like geomorphology, vegetation composition, microbial activity, temperature and moisture (Schuur et al., 2008; Harden et al., 2012). Organic carbon in permafrost origins from plant photosynthesis and growth. Low temperatures, anoxic conditions and limited drainage lead via cryoturbation, which transports OM to deeper horizons, to a carbon storage within the permafrost (Tarnocai and Stolbovoy, 2006; Bockheim, 2007; Schuur et al., 2008; Margesin, 2009; Obu et al., 2015). The carbon storage of permafrost is of great significance as permafrost soils contain more than twice the carbon contained in the atmosphere (Schuur et al., 2008). However, how much carbon is actually stored in permafrost is not yet fully known (Schuur et al., 2008). Hugelius et al. (2014) estimated for the northern circumpolar permafrost regions within a depth of 0-300 cm a carbon content of approximately 1035 Gt. Besides in high latitude landscapes, permafrost also exists in sub-sea and alpine areas (Romanovsky et al., 2007; Forbes et al., 2011). In Canada, more than half of the landmass is covered by permafrost that was formed during glaciation (Fig. 2.2).

In Alaska as much as 80 % of the landmass is permafrost. Permafrost is divided in continuous, discontinuous, sporadic as well as into isolated zones (Fig. 2.2). In total, continuous permafrost covers 90-100 % of the landscape affected by permafrost. Discontinuous permafrost underlies 50-90 %, sporadic permafrost 10-50 % and isolated permafrost less than 10 % of the landscape (French, 2007; Romanovsky et al., 2007). Both discontinuous and sporadic permafrost are characterized by a patchy permafrost distribution.

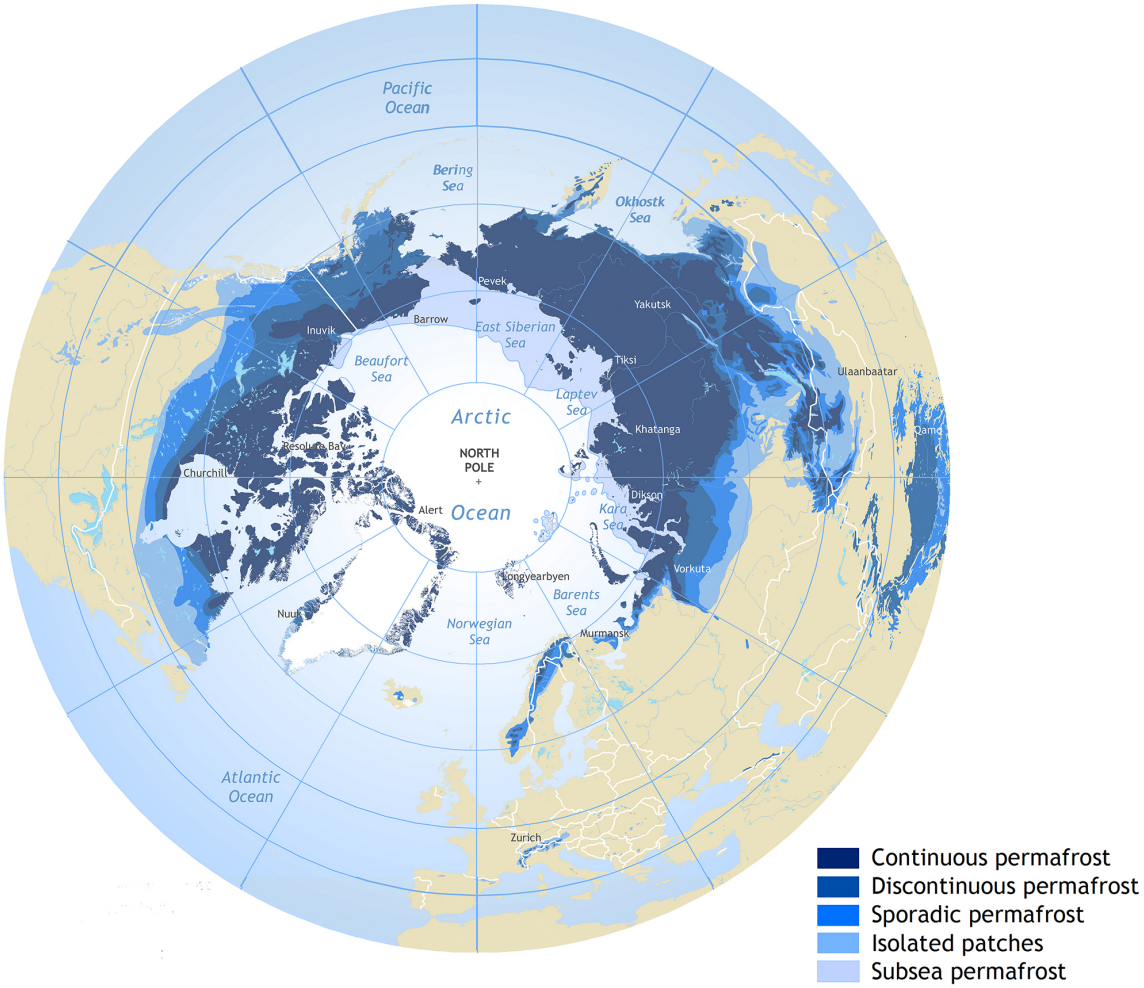

Figure 2.2: Distribution of permafrost in the northern hemisphere (according to Brown et al., 1997).

2.3 Ground Ice

Permafrost affected landscapes are characterized by ground ice. Ground ice is defined as all types of ice formed in freezing and frozen ground (Harris et al., 1988). In the Western Canadian Arctic the volume of ground ice is varying from some tenth to more than 80 % of the volume of the upper 30 m of the ground (Couture, 2010). Mackay (1972) classified ground ice based on the origin of water prior to freezing and water movement towards the freezing point. Not considered in the Mackay (1972) classification are buried ice types, such as glacier ice, snow bank ice, sea ice, river and lake ice. Later Mackay (1989) added a massive ground ice classification (Fig. 2.3). Massive ice is an extreme form of ground ice and refers

to ice with a gravimetric ice content greater than 250 % (Pollard, 1990). Mackay (1989) classified massive ground ice into two major categories, named buried ice such as surface ice and glacier ice, and intrasedimental ice such as ice-wedges, segregated ice and intrusive ice.

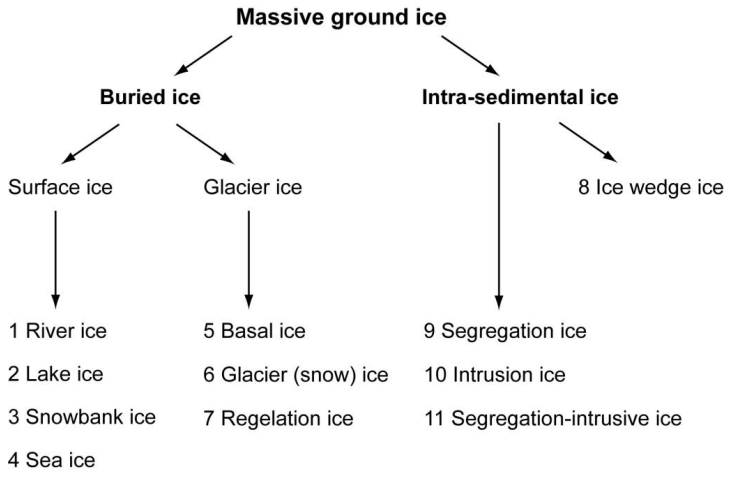

Figure 2.3: Massive ground ice classification (according to Mackay, 1989).

Intrasedimental, also named constitutional ice, forms by water that freezes in situ below the surface (Pollard, 1990). The North American classification by Mackay (1989) differs from the Russian ones, even though the Russians developed a ground ice classification first (Shumskii, 1959). Massive ice can be exposed in coastal outcrops or riverbanks (Fritz et al., 2011). Ground ice ablation leads to mass movements and to the growth of RTS (Fritz et al., 2011; Kokelj et al., 2013). Another form of ice is excess ice. Excess ice defines the volume of supernatant water that the ground would have under unfrozen conditions (Lantuit and Pollard, 2005; French, 2007).

2.4 Thermokarst

The term “thermokarst” describes the thawing of ice-containing permafrost, linked with “local or widespread collapse, subsidence, erosion, and instability of the ground surface” (French, 2007, p. 186) and affects the local morphology to a large extent (Oserkamp et al., 2009). Thermokarst occur by the thawing of ice-rich permafrost or the melting of massive ground ice (Lantuit and Pollard, 2005; Oserkamp et al., 2009) and are predominantly found in the Western Canadian Arctic (Lantuit et al., 2012), the Alaska Range (Jorgenson et al., 2001; Kanevskiy et al., 2013), and Siberia (Strauss et al., 2013). Thermokarst can affect carbon and nutrient

cycles by triggering the disposal of organic matter that has been frozen for thousands of years (Schuur et al., 2008; Abbott and Jones, 2015). Among the different features of thermokarst, RTSs are one of the most spectacular forms (Kokelj and Jorgenson, 2013). A RTS can be described as a type of erosional backwasting thermokarst, resulting from the exposure of ice-rich permafrost (Grom, 2008), initiated by mechanical erosion, fluvial processes, wave action (Couture et al., 2008) or by mass wasting due to extreme thawing of permafrost (Lacelle et al., 2010), and often occurs close to coasts or river banks. RTSs as dynamic thermo-erosional landscape features are characterized by a C-shaped depression and can be divided into the following areas (Fig. 2.4): 1) a nearly vertical "headwall" with an active layer (Fig. 2.4, B), 2) an inclined ice face below the headwall, with an angle varying between 20° and 50° (Fig. 2.4, C); 3) the slump floor at the base of the slump (Fig. 2.4, A), separated into a mud pool, vegetated areas, and mud lobe discharging the slump (Burn and Lewkowicz, 1990; Lantuit and Pollard, 2005; Kokelj and Jorgenson, 2013).

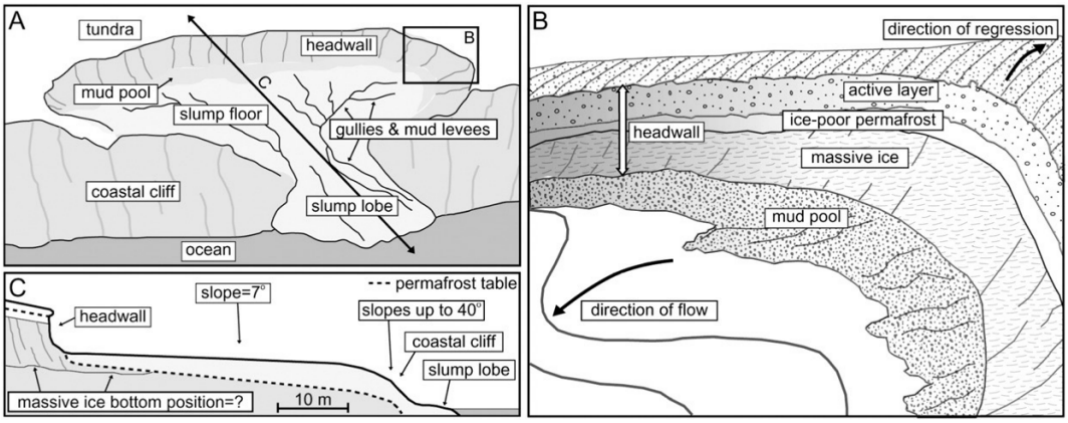

Figure 2.4: Sketch for RTS, (A) overview of a RTS, (B) profile of a slump headwall, (C) crossection of a slump (according to Lantuit and Pollard, 2005).

Headwalls of RTS can be up to 20 m high and expose massive ice bodies (Harris et al., 1988; Lantuit and Pollard, 2008). The stability of the headwall depends on size and orientation of the headwall, of the ground ice content and of the surface energy fluxes. A loss in stability results in the growth of RTS. The exposed ice at the headwall is susceptible to insolation and heat transfer by wave action, from water flowing over the headwall (Grom, 2008). The waves crashing against the headwall or the slump floor can cause salt efflorescence (Kokelj and Lewkowicz, 1999). As a consequence the ice face thaws. Not only the headwall but also the active layer is affected by environmental forcing. Warmer air temperatures and a warming permafrost result in the deepening of the active layer. With a headwall retreat the active layer collapses and material gets added to the mud pool. The supersaturated sediment can

accumulate at the slump floor (Lacelle et al., 2010) or flow into the Arctic shelf sea right away by enhanced gullying (De Krom, 1990; Robinson, 2000; Lantuit and Pollard, 2008; Kokelj et al., 2015), which causes high sediment concentrations in the adjacent lake, stream or ocean (Bowden et al., 2008) and has the capability to alter the nearby ecosystem (Kokelj et al., 2009). RTS are usually polycyclic, which means more than one slump generation can be identified within a RTS (Lantuit et al., 2012). This phenomenon is linked to coastal or shore erosion and changes the physical properties of the sediment (Lantuit et al., 2012), which may lead to exposed ground ice (Lantuit and Pollard, 2008). Stabilised RTS occur when the ground ice has melted or the headwall gets protected by slumped material (Burn and Lewkowicz, 1990; Lantuit et al., 2012). Stabilised areas within a RTS reestablishes a new vegetation cover, different from the surrounding tundra (Lantuit et al., 2012).

2.5 Arctic permafrost and environmental forcing

Unlike temperate coasts, Arctic coasts are affected by the presence of ice, as sea ice in the marine area and as ground ice in the permafrost, making them particularly vulnerable to environmental forcing (Rachold et al. (2005); Lantuit et al. (2011, 2012a), Fig. 2.5). Further, 65 % of the Arctic coasts are composed of unlithified material, which makes them additionally vulnerable to erosion (Lantuit et al., 2012a). Environmental forcing include i. a. air temperature, ocean temperature, permafrost temperature, storms, waves and sea ice (Fig. 2.5).

According to Walsh et al. (2011), with a higher air temperature the permafrost temperature increases, the snow cover decreases, the sea ice extent decreases, the ice break-up begins earlier, the sea level rises and precipitation increases. An example for permafrost temperature increase is i. a. the Mackenzie Delta, where a warming of 0.6 °C at a depth of 24 to 29 m between 1989 and 2003 was detected (Smith et al., 2005). The total extent of permafrost thaw is still unknown. The study of Lawrence and Slater (2005) suggests that the near-surface permafrost may decrease by 90 %, from 10.5 million km² to 1.0 million km² by the end of this century. Other calculations regarding the permafrost thaw extent by 2100 provide a value between 40 to 80 % permafrost loss (Lawrence and Slater, 2005; Saito et al., 2007; Lawrence et al., 2011). As a consequence of an increasing permafrost temperature the permafrost retreats and thus influences the morphology of permafrost affected terrain. For example, Lantuit and Pollard (2008) observed that coastal erosion is highest where RTS occur due to exposed ground ice. With eroding permafrost coasts sediment and OM get released into the nearshore zone or into

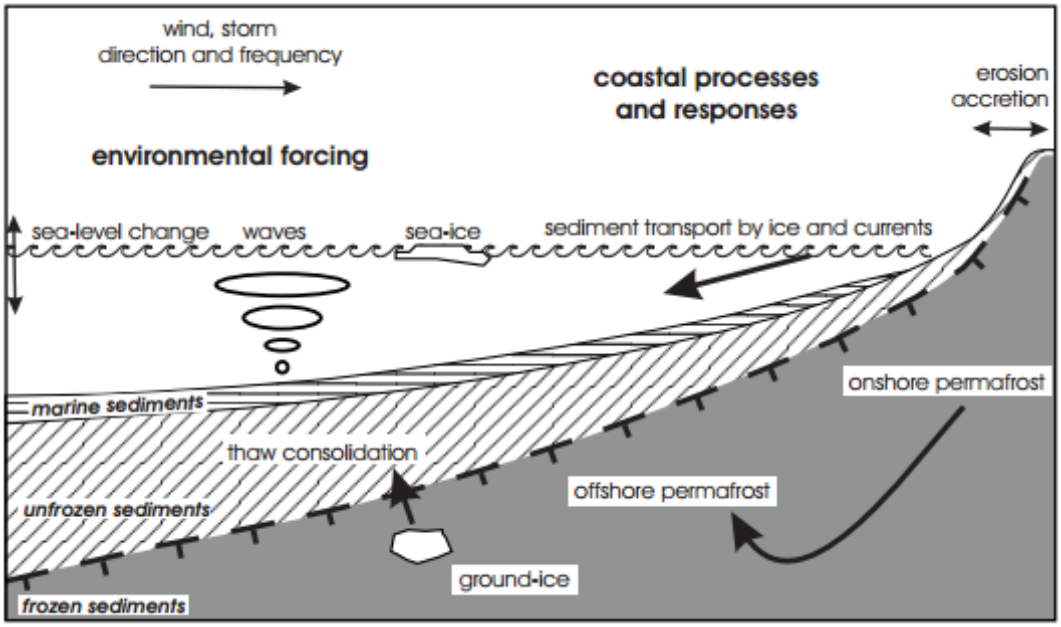

Figure 2.5: Sketch of environmental forcing affecting Arctic permafrost coasts and responses of the Arctic coast (according to Rachold et al., 2005).

the atmosphere (Rachold et al., 2005), which impacts the coastal ecosystem and contributes to the greenhouse gases (Kokelj et al., 2009).

Storms have the strongest impact on the coast during the ice-free season between June and August (Atkinson, 2005; Solomon, 2005), because during this period the coast is not protected by sea ice. These strong winds transport the material as well as strengthen the waves by transferring energy to the water (Lantuit and Pollard, 2008). Due to the decreasing sea ice caused by climate warming storms and wave action affect the coast until the late fall (Atkinson, 2005). The waves, induced by storms, interact with the coast resulting in sediment transportation and erosion (Lantuit et al., 2012a). With a warmer ocean water temperature the waves also have a higher influence in affecting the ground temperature and the salinity of the ground.

Sea ice, as another important factor, insulates the relatively warm ocean water from the cold polar atmosphere, absorbs incoming radiation and regulates exchanges of heat, moisture and salinity but also transports sediments. During the summer, wave action is substantially dampened by sea ice floes, but during spring, autumn and winter wave action is limited by the presence of sea ice cover (Atkinson, 2005; Forbes et al., 2011; Lantuit et al., 2012a). With higher surface air temperatures (SAT), the thickness and volume of sea ice decreases (Rothrock and Zhang, 2005; Serreze and Stroeve, 2015; Wood et al., 2015). With less sea ice extent the ocean

absorbs incoming radiation and thus gets warmer (Allard and Pollard, 2011; Günther et al., 2015). The warmer ocean temperature leads to a later sea ice formation, including a longer open water season with waves having a longer time period to impact on the coast (Günther et al., 2015).

2.6 Study area

2.6.1 Herschel Island

Herschel Island (69°36'N; 139°04'W), also known as Qikiqtaruk, meaning "this is the island" in Inuvialuktun, is part of the Yukon Territory, Canada, located in the southern part of the Beaufort Sea (Arctic Ocean) and is Canada's westernmost Arctic island (Fig. 2.6).

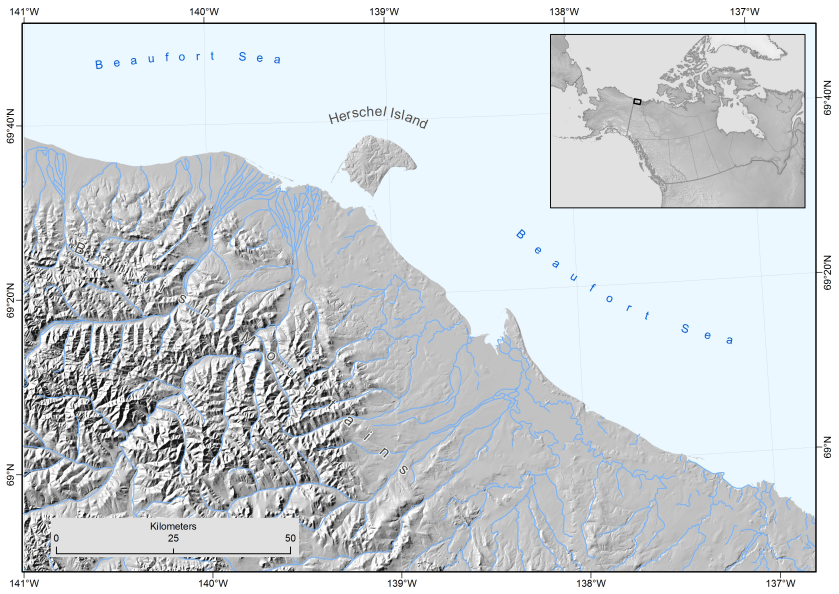

Figure 2.6: Location of Herschel Island situated in the Northern Canadian Arctic.

Herschel Island is situated 2 km offshore the Yukon coast, which extends from the Mackenzie Delta in the east to the Alaskan boarder in the west. It has an area of 108 km² and a coastline length of 60 km (Fritz et al., 2011). The Yukon coast is one of the most ice-rich permafrost coasts in the Canadian Arctic (Lantuit and Pollard, 2005; Lantuit et al., 2012), with permafrost reaching depths of up to 600 m (Pollard, 1990; Smith and Burgess, 2000). The shelf area of the Yukon coast is characterized by two depressions, the Mackenzie Trough, a submarine canyon, and the Herschel Basin. During the Late Wisconsin glaciation the Laurentide Ice

Sheet covered large parts of northern Canada including Herschel Island (Mackay, 1959). With the ice-sheet reaching its maximum extent during the Buckland Stage, an early stage of the Wisconsin Glaciation, frozen sediments got pushed up and formed Herschel Island (Mackay, 1959). Since deglaciation, Herschel Island remains in the Beaufort Sea as an ice thrust moraine with a rolling topography (Pollard, 1990). With rising sea level in the Holocene, the island got separated from the mainland (Burn, 2012). The deposited sediments, like marine clay, silt and occasionally sand (Bouchard, 1974) are affected by permafrost. Postglacial deposits consist of organic matter, litter and alluvial sediments (Fritz, 2008). In the winter the southern Beaufort Sea is frozen and sea ice covers the coast of Herschel Island, but during summer months the ice-rich coast is accessible for environmental forcing, especially for storms and waves (Atkinson, 2005; Lantuit and Pollard, 2008). Due to the climate warming a decrease in the sea ice extent is already detectable (Fetterer et al., 2002; Stroeve et al., 2012; Serreze and Stroeve, 2015). This leads to an unprotected coast for not just the three summer months but for a longer time period.

2.6.2 Permafrost and geomorphology

Herschel Island is situated in a region of continuous permafrost, with a mean annual ground temperature of -8 °C (Burn et al., 2004). With a glacial origin and thus a very ice rich permafrost coast, plus consisting of unlithified sediments, Herschel Island is very vulnerable to a warmer SAT, a warming permafrost as well as a warming ocean, which have the power to alter Herschel Islands morphology. There is a manifold spectre of ground ice on Herschel Island, including ice wedges, relict glacier ice, and ice lenses. The sediments of Herschel Island are in general fine grained silt to clay with sand and gravel contents. In the summer months from June to August the upper surface layer (active layer) thaws up to 55 cm in depth (Burn and Zhang, 2009) and refreezes in the winter months. On Herschel Island approximately 3.9 Tg of soil organic carbon and 0.4 Tg of total nitrogen are stored in the top meter of permafrost (Obu et al., 2015). The morphology of Herschel Island is dominated by rolling hills, polygonal ground, block failures, RTS and active layer detachment slides (Lantuit and Pollard, 2008; Burn, 2012). The island has alluvial fans, like the Pauline Cove, and fluvial streams, which transport sediments to the ocean by gullys (Burn, 2012). The north and north-west side of Herschel Island is characterised by bluffs, with heights of up to 60 m (Burn, 2012). The south-east side of the island shows the highest concentration of RTS. From 1950 to 2000 the number of thaw slumps on Herschel Island increased by 125 %, their total area by 160 % (Lantuit and Pollard, 2008). From 1954 to 1970 and from 1970 to 2000 the coasts eroded with rates of

0.61 m/yr, and 0.45 m/yr, respectively. Highest erosion rates occur on the south and south-east coast of Herschel Island (Lantuit and Pollard, 2008).

2.6.3 Climate and vegetation

The climate on Herschel Island is Arctic maritime, with winters lasting for about 250 days and short summers with 24 h of sunlight a day (Cray and Pollard, 2015). The maximum daily mean temperature measured 2011 during July reached 16.8 °C, and the minimum during January reached -39.8 °C (Canada, 2012). The mean annual temperature is around -11.3 °C (Burn and Zhang, 2009; Margesin, 2009). The islands mean annual precipitation is 160 mm (Canada, 2012). About 70 % of the annual precipitation occurs during the summer as rain (Burn and Zhang, 2009), with August being the rainiest month of the year due to the ice-free Beaufort Sea (Cray and Pollard, 2015). The snow depth in the late winter is about 20 cm thick (Burn and Zhang, 2009). Herschel Island is affected by strong winds, which are continental in winter and maritime in summer. The wind speeds measured during 2009 to 2012 reached a maximum of 67 km/h (Radosavljevic et al., 2015). The wind speed and direction can play a role for erosion dynamics and thus play an important role for Herschel Island, especially in the ice-free summer season (Lantuit and Pollard, 2008). North-westerly winds, which are present for most of the year, cause a positive surge (Radosavljevic et al., 2015). In the summer the wind turns (Bouchard, 1974) and induces a negative surge (Radosavljevic et al., 2015). The Yukon coast is situated 100 km north of the modern tree line and is covered by tundra. On Herschel Island, tussock tundra, an Arctic lowland tundra, is present with cotton grass (Eriophorum spp.) as a dominant vegetation type (Myers-Smith et al., 2011; Sloan and Pollard, 2012). Other commonly found vegetation types are dwarf shrubs, sedges, grasses, mosses and lichens (Cray and Pollard, 2015). Dwarf willows can be found on steeper upland slopes. Water sedges and willows grow on alluvial fans. Active slumps show next to non-vegetated areas also areas with graminoids and forbs (Cray and Pollard, 2015). Stabilized footslopes of RTSs on Herschel Island are colonized by plants like grasses, marsh ragwort, sea-shore chamomile, Tilesius' wormwood and mosses (Kennedy, 2012). Cray and Pollard (2015) show between 0 and 20 years of stabilisation for a RTS on Herschel Island, vegetation of low diversity, mostly grass-dominated vegetation, and after a few hundreds of years forb, dwarf shrub, and litter.

2.6.4 Study sites

This study focusses on the RTS "Slump D" along the south-east coast of Herschel Island. Sampling took place during the expedition "Yukon Coast 2014" from July to August. The maximum height of Slump D reaches up to 50 m above sea level. The slump is more than 400 m in width and has a vertical headwall of approximately 10 m height (Fig. 2.7).

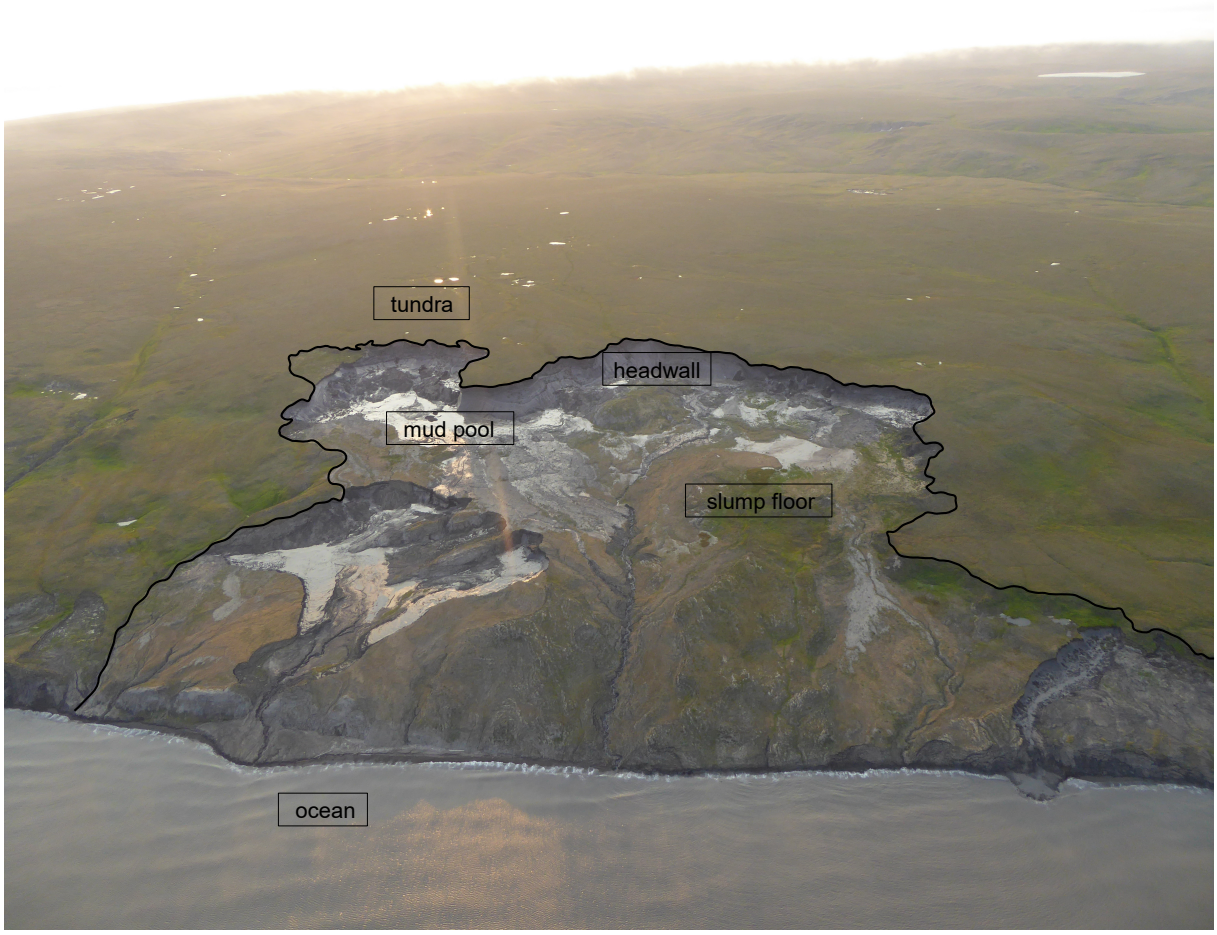

Figure 2.7: Aerial view of Slump D on Herschel Island. Solid line shows extent of Slump D. Named squares show the different zones of Slump D: the tundra surrounding Slump D, the headwall of Slump D, shiny areas show the mud pool, dry areas show the slump floor (Photo: I. Eischeid (2015)).

Tundra, in form of a hummocky terrain, is surrounding Slump D. Massive ground ice exposed on its headwall is most likely basal regelation glacier ice, showing glaciotectonic deformation structures (Fritz et al., 2011). Slump D owns a very complex RTS system, because of its active and non-active areas, and its mud pools. For this study Slump D was divided in two main zones, an undisturbed zone with 1) the tundra zone and 2) the permafrost zone, and a disturbed zone with 3) the mud pool zone and 4) the slump floor zone. In samples for the tundra zone were taken in a depth of 10 and 30 cm. At three permafrost profiles within the headwall sediment samples have been taken, representing the permafrost zone. The mud pool and the slump floor zone were sampled on the surface and in 10 and 30 cm depth. With ArcGIS 10.1 a fishnet grid was applied to the whole slump zone to guarantee representative and unbiased sampling (Chap. 3.3).

3 Methods

All samples taken on Herschel Island have been processed and analysed in the geochemical laboratory of the Alfred Wegener Institute, Helmholtz Centre for Polar and Marine Research (AWI) in Potsdam, Germany and at the German Research Centre for Geosciences (GFZ) in Potsdam, Germany. Laboratory analysis included biogeochemical parameters (total carbon (TC), total organic carbon (TOC) and total nitrogen (TN)), and stable organic carbon isotopes ($\delta^{13}C_{org}$) of 100 samples. Fig. 3.1 shows the process of sample-treatment after field work.

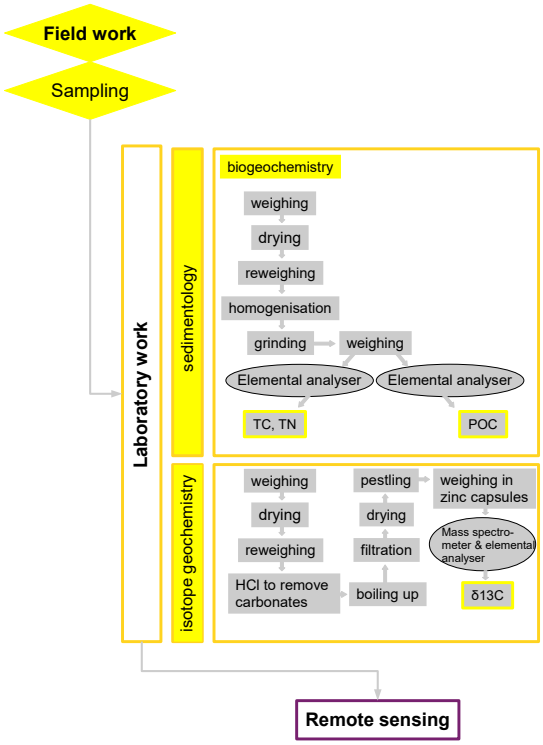

Figure 3.1: Summerising scheme of methods and preparation used for all samples.

3.1 Field Work

Field work took place on Herschel Island during the AWI Expedition “Yukon Coast 2014”. The RTS “Slump D” is one of the biggest slumps in the Arctic and was primarily chosen due to the availability of pre-existing datasets and safe accessibility. Further, it is important to consider that the samples were taken during the summer months July and August. Here the slumping process is highest because of the warmer air temperatures and the open water season. During sampling field descriptions of the topography, aspect, relief, height of exposure, elevation and dimension of the slump, surrounding vegetation, as well as interpretation of landform and geomorphological processes were written into the fieldbook. Geographical coordinates were recorded by a Garmin etrex Legend Hcx handheld GPS. To ensure pristine samples the thawed surface of the permafrost zone was removed before the samples were taken. The tundra zone was sampled in a depth of 10 and 30 cm. Representative for the permafrost zone sediment profiles were taken along the headwall in different depths, to cover all stratigraphical units. Samples for the permafrost profile 1 were taken at a depth of 40, 90, 120, 150, 190, 220 and 250 cm. For permafrost profile 2 samples were taken from 100, 150 and 190 cm depth. Permafrost profile 3 was sampled at a depth of 90, 130, 180, 220, 260 and 340 cm. The mud pool zone as well as the slump floor zone were sampled in a depth of 0, 10 and 30 cm. A fishnet grid was applied on a GeoEye-image of Slump-D from 2011 in order to define representative sampling locations (Fig. 3.2).

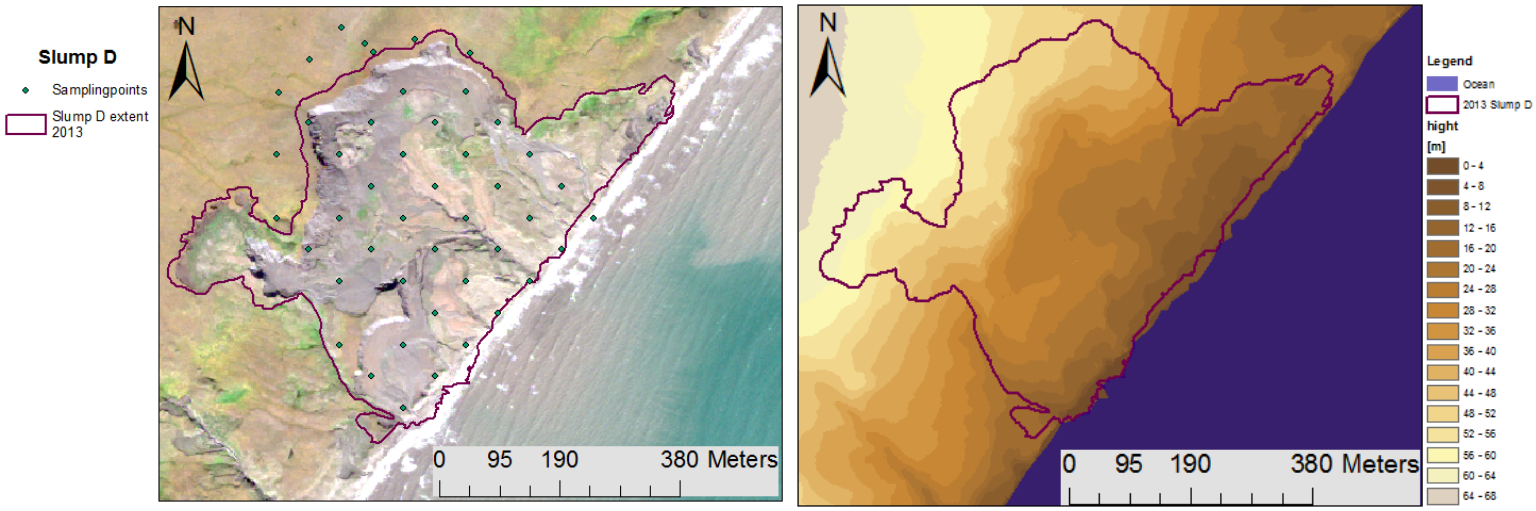

(a) fishnet grid

(b) DEM

Figure 3.2: (a) fishnet grid applied on a GeoEye-image showing samplelocations, (b) heights along Slump D.

Each sample was put into Whirl-Pak bags and named according to a standard nomenclature, like SlpD14-TS-F8-01, where SlpD stands for Slump D, in year 2014 (14), in the thaw slump (TS), with the sample number F8, in a depth of 10 cm (1). The samples for the permafrost zone were named as permafrost 1 (PS1), permafrost 2 (PS2) and permafrost 3 (PS3). To keep samples frozen they were transported in a thermobox. Back in Potsdam the samples were stored in a freezer at -20 °C until processing in the lab. The tundra and slump samples were taken by a cylinder with a known volume (200mm³). The permafrost profiles were taken from the headwall of Slump D with a Hiltidrill. Samples were stored in a Whirl-pak bag and then right into a thermally isolated box in an ice house at approximately -8°C on Herschel Island until transfer to Potsdam.

3.2 Laboratory methods

TC, TOC as well as TN were measured at the AWI, Potsdam, Germany. $\delta^{13}C_{org}$-values were analysed at the GFZ, Potsdam, Germany. In total 100 soil samples (n = 100) were analysed. All samples were controlled thawed at 20°C, weighed, freeze-dried and weighed again. After drying samples were homogenised by using a ceramic grinder.

3.2.1 Biogeochemistry: Measurement of TC, TOC and TN

For the TC- and TN-analyses 8 mg of each homogenized sample were extracted twice and put into zinc capsules. At the beginning and at the end of each measuring day, a blank capsule for background detection was used to test for potential inaccuracies in the measurements. Control and calibration standards were measured along with the samples. The control standards are used to ensure the accuracy of the device of ± 0.1 wt%. The samples were measured by a CN elementar analyser (Handbook, 2005). The analyser measures the samples by the principle of catalytic tube combustion at >900 °C. The capsules were released to the analyser via sample disposer. In an oxygenated CO_2 environment the carbon and nitrogen get oxidised explosively. Helium (He) works as a carrier gas for the remaining components CO_2 and N_2. Distinctive components detected by a thermal conductivity detector get separated by specific adsorption columns, here carbon (Handbook, 2005). In the end the percentage of TC and TN are calculated from its absolute gravimetric content compared to the input sample weight. The detection limit is <0.1 %.

3.2.2 Biogeochemistry: Measurement of TOC

For the TOC analysis, a similar procedure was used. Samples were measured with the elementar analyser, "vario MAX C", working with an IR detector. Blank capsules were used at the beginning and at the end of each measure-day to guarantee correct measurements. Standards were used to ensure the accuracy of the device. The combustion took place at a temperature of around 550 °C. With the combustion, carbon got transferred into CO_2. The detection limit is <0.1 %.

3.2.3 Stable isotope geochemistry - Carbon isotopes($\delta^{13}C_{org}$)

For the analysis of $\delta^{13}C_{org}$ 3 gram of each freeze-dried sample was weighed in an Erlenmeyer flask. Then 20 ml HCl (of 1,3 mol/l) were added to remove all carbonate. Subsequently the sample in the Erlenmeyer flask got warmed up to 98 °C. After three hours on the hot plate the Erlenmeyer flask was filled up with distilled water. For three days in a row the flask was filled up again with distilled water to wash out the HCl. After three days the samples were filtered with a 1.0 µm glass microfiber filter using a vacuum pump and dried afterwards. Thereafter, the dried samples got grinded and weighed into tin capsules. With the help of TOC-measurements the amount of sample for $\delta^{13}C_{org}$-measurements was estimated according to the following formula:

$sampleweight[g] = \frac{20}{TOC}$

The carbon isotope $\delta^{13}C_{org}$ was determined by isotope ratio mass spectrometry (IRMS). Therefore, the tin capsules were inserted into the Elementar analyser DELTAplusXL Finnigan (ThermoFisher Scientific). The elementar analyser works with the CarloErba Elementar Analysator NC2500 with an analytic precision of < 0.2 ‰. All samples were combusted at a temperature of around 950 °C. By the carrier gas helium, the samples get transported into the chemical trap, where water gets removed. During the next step CO_2 and N_2 get separated (Muccio and Jackson, 2009). A standard gas of known isotopic composition, in this case CO_2, is measured against the sample gas so that the isotopic ratio can be calculated. CO_2 gets ionised in the ionisation chamber, accelerated and focused in an electronic field inside the mass spectrometer. A magnetic field separates the ions depending on their mass. The separated ion beams get detected by the three Faraday-collectors, a metal cup in a vacuum, which collects ions. In total three ion beams corresponding to CO_2 with an atom mass of 44, 45 and 46 were measured by the Faraday-collectors (Fig. 3.3).

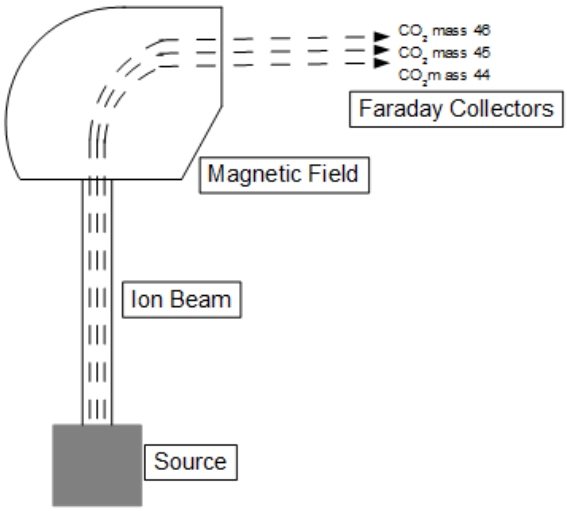

Figure 3.3: IRMS, simplified sketch. Source producing ion beam, magnetic field seperates the ions, which get detected by the Faraday Collectors.

These ions produce an electrical current, which is proportional to the total number of ions inside the cup. With the known released specific electrical currents, the $^{13}C/^{12}C$-ratio (= R) can be calculated, reported as ‰-differences against the international reference standard Vienne Pee Dee Belemnite (VPDB; Craig, 1953):

$$\delta^{13}C_{sample} = [\frac{R_{(sample)}}{R_{(standard)}} - 1] \cdot 1000\ ‰$$

3.3 Remote Sensing

The retrogressive thaw slump “Slump D” was divided into the four different zones based on a GeoEye image from 2011. The image has a nominal collection azimuth of 220.6 degrees and a nominal collection elevation of 82.2 degrees, and was available at AWI, Potsdam. The GeoEye image has a resolution of 1.65 m, suitable for the purpose of this study. The GeoEye was the best available image for this scale. Although sampling took place in 2014, 2 years after the picture was taken, the image fulfilled its purpose to select representative and non-biased sampling locations using a fishnet method with ArcGIS. Size and dimension of the slump changed during the two years but do not affect the analysis as field notes have been taken to assign every sample location to the sample point, even if they have changed during the years.

4 Results

For each sample the biogeochemical parameters TC, TOC, TN as well as the stable isotope $\delta^{13}C_{org}$ have been measured. The results are summarized in this chapter. The four zones are shown in Fig. 4.1. Within the mud pool, surface samples have been taken where it was not possible to dig holes. First all zones are examined separately and then compared, in order to detect significant differences in carbon and nitrogen concentrations between undisturbed and disturbed zones. The complete dataset with coordinates can be found in the Appendix.

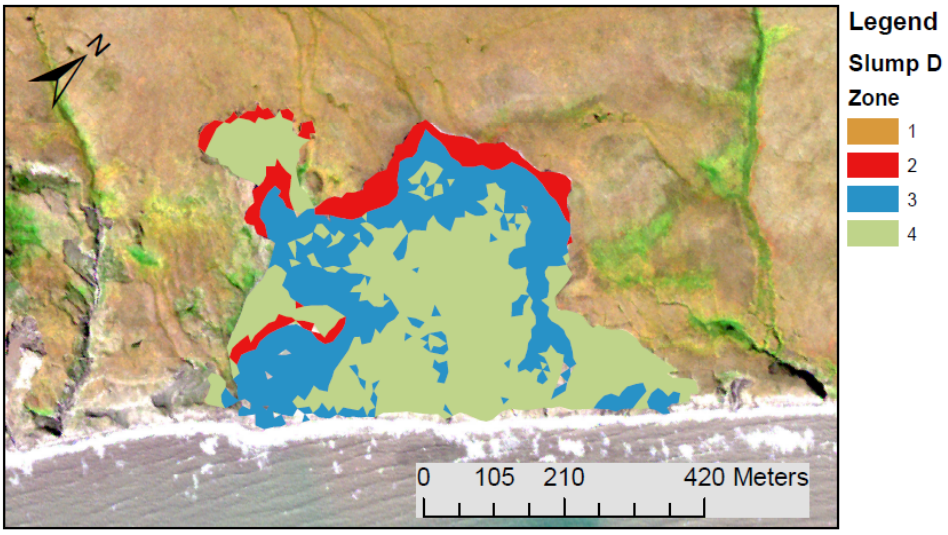

Figure 4.1: Zones for Slump D, in yellowish: tundra zone (1), in red: permafrost zone (2), in blue: mud pool zone (3), in green: slump floor zone (4).

4.1 Undisturbed zone

4.1.1 Tundra zone

The hummocky terrain of the tundra zone is covered nearly completely with vegetation (90 to 100 %). The sediment of the tundra zone is composed of greyish silty clay with some gravel and peat layers and is well-rooted up to approximately 20 cm depth (Fig. 4.2). In total 11 samples have been taken (n=11).

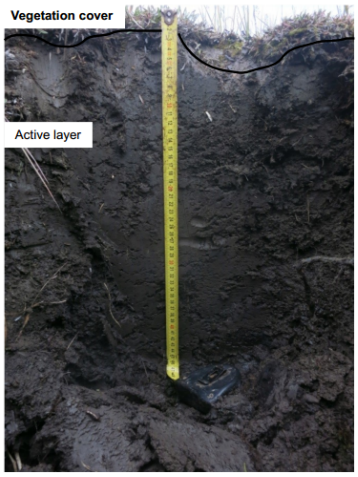

Figure 4.2: Representative profile for the tundra zone, measuring tape shows 45 cm in depth (Photo: G. Tanski (2014)).

Table 4.1: Data for tundra showing number of samples, range of values, average value and median.

	TC [%] 10cm	TC [%] 30cm	TOC [%] 10cm	TOC [%] 30cm	TN [%] 10cm	TN [%] 30cm
No. of samples	5	6	5	6	5	6
Range	2.5 - 9.6	1.8 - 9.6	1.4 - 9.0	0.6 - 9.7	0.1 - 0.8	0.1 - 0.7
Average	6,1	4,6	5,4	4,1	0,5	0,3
Median	4,8	3,6	4,5	3,0	0,4	0,3

	TOC/TN 10cm	TOC/TN 30cm	δ13Corg [‰] 10cm	δ13Corg [‰] 30cm
No. of samples	5	6	5	6
Range	12.0 - 15.6	6.4 - 16.3	-26.5 - -26.9	-25.3 - -27.6
Average	13,5	12,4	-26,7	-26,7
Median	13,1	13,0	-26,7	-26,7

The TC-values in 10 cm depth range from 2.5 to 9.6 %, with a mean value of 6.1 %. The TOC-values range between 1.4 and 9.0 %, with a mean value of 5.4 %. For TN, values range between 0.1 and 0.8 % and show a mean value of 0.5 %. The TOC/TN-ratio ranges between approximately 12.0 and 15.6 (Tab. 4.1). The mean value is 13.5. The $\delta^{13}C_{org}$-values are very similar distributed with a mean value of -26.7 ‰, ranging from -26.9 to -26.5 ‰ (Tab. 4.1). The TC-values in 30 cm depth are between 1.8 to 9.6 %, with a mean value of 4.6 %. The TOC-values range from 0.6 to 9.7 %, and show the highest TOC-value measured for all tundra samples. The mean TOC-value is 4.1 %. TN shows values of between 0.1 and 0.7 % with a mean of 0.4 %. The TOC/TN-ratio shows values from 6.4 to 16.3 and 12.4 as the mean value. The $\delta^{13}C_{org}$-values show amounts from -27.6 to -25.3 ‰, with a mean value of -26.7 ‰. In total, the upper part of the tundra (10 cm) shows higher TC-values than the lower part (30 cm), with a difference of 1.5 %, when comparing the mean values. The mean TOC-values differ by 1.3 %, with higher values in a depth of 10 cm. The mean TN concentrations differ by 0.1 % and are thus higher in the upper part at 10 cm (Tab. 4.1). In contrast, the TOC/TN-mean-ratios differ by 1.1 %, with a higher mean value at 10 cm depth. But in the upper 10 cm the minimum of TOC/TN is 12 and thus two times higher than the minimum for 30 cm. The $\delta^{13}C_{org}$-mean-values do not differ between 10 and 30 cm. At a depth of 10 cm $\delta^{13}C_{org}$-values show the lowest value of -27.6 ‰, at a depth of 30 cm the highest value of -25.3 ‰ has been measured, which is the highest value of $\delta^{13}C_{org}$ measured in total.

4.1.2 Permafrost zone

The permafrost profiles represent different zones within the slump headwall and differ in their TC, TOC and TN content.

Permafrost profile 1 is separated in 4 stratigraphic units. On top is an active layer (unit 1) with a thickness of 26 cm (Fig. 4.3). Below the active layer an ice-rich diamicton with a depth of 224 cm follows. The ice-rich diamicton, consisting of sandy-silty sediment, reveals 2 different units. The first one (unit 2), reaching from 26 cm to 180 cm shows peat intrusions with up to 15 to 20 cm in diameter as well as ice lenses of 1 cm thickness. Next to the ice lenses round air bubbles of 1 to 5 cm in size occur at the lower part of the first unit. In unit 3, reaching from 180 to 250 cm, thicker ice lenses of 5 to 10 cm can be found with less peat intrusions (Fig. 4.3). An active layer debris (unit 4) completes the profile.

For permafrost profile 1 7 samples (n=7) were taken. The TC-values show a mean value of 10.6 %, where values decrease with increasing depth from 16.9 to 4.6 %, but show a discon-

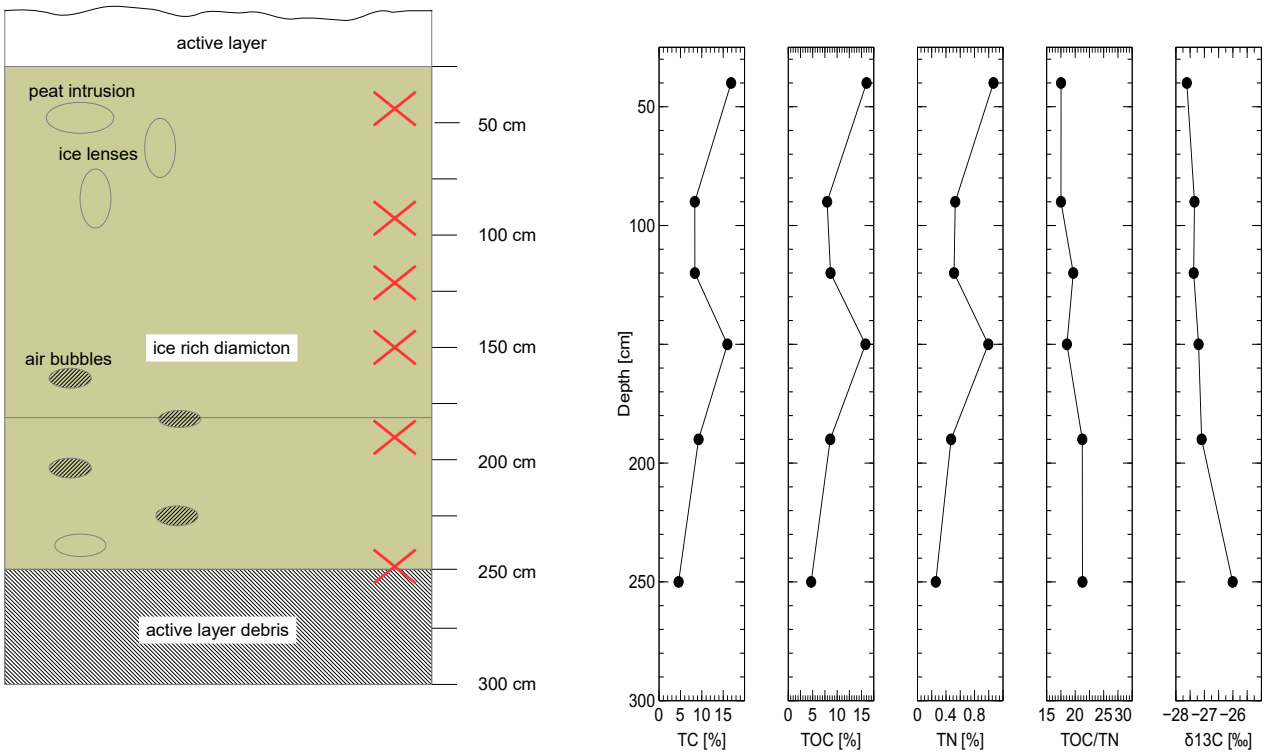

(a) Sketch (b) Data

Figure 4.3: (a) Sketch: red crosses show sample points, (b) data for permafrost profile 1: summary of biogeochemical and stable isotope parameters.

Table 4.2: Data for permafrost profile 1 along its depth from 40 cm to 250 cm.

Depth [cm]	TC [%]	TOC [%]	TN [%]	TOC/TN	δ13Corg [‰]
40	16,9	16,0	1,1	15,8	-27,6
90	8,4	8,0	0,5	15,8	-27,3
120	8,4	8,6	0,5	16,3	-27,4
150	16,0	15,8	1,0	16,1	-27,2
190	9,2	8,6	0,5	19,6	-27,1
220	10,6	11,5	0,5	19,7	-26,9
250	4,6	4,7	0,3	17,8	-26,0

tinuity at 150 cm depth with a value of 16.0 % (Tab. 4.3). This discontinuity occurs at the transition from section 2 to section 3 within the ice-rich diamicton, where a change of air bubbles and peat intrusion takes place. The highest TOC-values are in the first 40 cm of permafrost profile 1 of around 16.0 %. With increasing depth (> 40 cm) the TOC values decrease from 8.0 to 4.7 %. The mean value for TOC is 10.3 %. The same discontinuity as seen for

TC can be seen for TOC and TN. TN and $\delta^{13}C_{org}$ are the highest in PS1-01 with contents of around 1.1 % and -27.6 ‰. TN shows at the discontinuity at 150 cm a value of around 1.0, but in total decreasing contents from 1.1 to 0.3 % with increasing depth. The mean value of TN is 0.6 %. The TOC/TN-ratio increases until 250 cm depth from 17.5 to 21.3 but shows a discontinuity at 120 cm depth, with a value of 19.7. Its mean value is 19.3. $\delta^{13}C_{org}$ decreases with a starting value of -27.6 ‰continuously with depth and is the highest at 250 cm with -26.0 ‰ (Fig. 4.3). The discontinuity found for TOC/TN correlates with $\delta^{13}C_{org}$. At 120 cm $\delta^{13}C_{org}$ shows a value of -27.4 ‰. The mean value is -27.1 ‰.

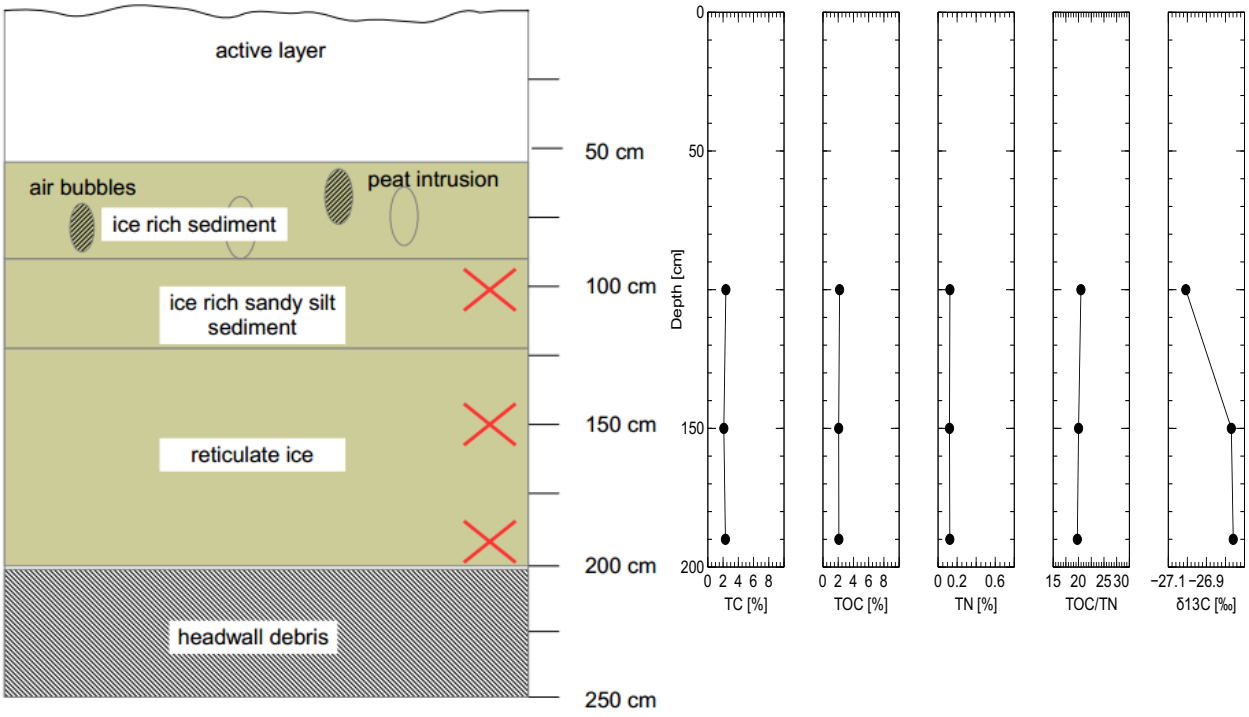

(a) Sketch (b) Data

Figure 4.4: (a) Sketch: red crosses show sample points, (b) data for permafrost profile 2: summary of biogeochemical and stable isotope parameters.

Permafrost profile 2 is separated into 5 untis, showing a depth of 190 cm. The first unit, the active layer, has a depth of 0.56 cm. In the second unit from 0.56 to 0.85 cm ice rich sediments with a reticulate ice cryostructure and air bubbles are prominent. Ice rich sandy-silty sediments with peat intrusions can be found in the third unit at 0.85 to 120 cm. The fourth unit, reaching from 120 to 200 cm shows reticulate ice in a sandy-silty sediment. The permafrost sediments are underlain by massive ice, that is covered in a debris of thawed permafrost sediments and tussocks (unit 5) (Fig. 4.4).

Table 4.3: Data for permafrost profile 2 along its depth from 100 to 190 cm.

Depth [cm]	TC [%]	TOC [%]	TN [%]	TOC/TN	δ13Corg [‰]
100	2,4	2,2	0,1	19,0	-27,0
150	2,1	2,1	< 0,10	21,0	-26,8
190	2,3	2,1	0,1	18,7	-26,8

For permafrost profile 2 3 samples (n= 3) were measured. The three samples were taken in 100, 150 and 190 cm depth (Fig. 4.4). TC, TOC as well as TN show at a depth of 150 cm lower values than in 100 and 190 cm. TC-values range between 2.4 to 2.1 %, with a mean value of 2.3 % (Tab. 4.3). At 150 cm it shows a value of 2.1 %. TOC shows similar values of 2.2 to 2.1 %, with a mean value of 2.1 %. At 150 cm is shows 2.1 % TOC. TN has a mean value of around 0.1 %, at 150 cm the TN-content was too low to be detected. The TOC/TN-ratio ranges between 20.5 and 19.8, with a mean value of 20.1. $\delta^{13}C_{org}$ shows values from -27.0 to -26.8 ‰, with am mean value of -26.8 ‰.

Permafrost profile 3 is separated into 6 units (Fig. 4.5). Unit 1, the active layer of permafrost profile 3 (PS3), is 0.37 cm thick. Unit 2, which stretches down to 150 cm is composed of ice-rich sediment with a reticulate ice structure, including peat intrusions, ice lenses with thickness > 20 cm and air bubbles. At 150 cm to 240 cm, unit 3, an ice rich diamicton with an irregular reticulate ice and brownish-yellowish sediment bands is present. Unit 4 from 240 to 330 cm is characterised by ice-rich, sandy-silty-clay sediment with ice lenses and shell fragments. From 330 cm down to 350 cm a layer with structureless ice follows. Below the exposed permafrost sediments, massive ground ice, unit 5, concludes the profile.

For permafrost profile 3 6 samples (n = 6) were measured. TC-values decrease with depth from 4.6 to 1.4 %, with a discontinuity at 220 cm showing a value of 3.1 % (Fig. 4.5). The discontinuity occurs at the transition from unit 3 to 4. The mean value for TC is 2.7 %. TOC-values vary within the permafrost profile. Highest TOC-values with 4.7 % have been found in a depth of 90 cm. At a depth of 180 cm, the TOC-values decrease from 3.5 to 0.9 % and increase further up to 3.3 % in 220 cm depth (Tab. 4.4). The same discontinuity at 220 cm as found in the TC-values is detectable. From this depth on TOC proceed to decrease again until 340 cm to 1.3 % (Fig. 4.5). Its mean value is 2.5 %. TN-values decrease from 0.3 % at 90 cm to 0.2 % at a depth of 130 cm. Beneath 130 cm the values are below detection limit. The mean value for TN is 0.2 %. The TOC/TN-ratio is 22.3 at 90 cm depth and decreases to 19.1 at 130 cm depth. For sediments below 130 cm no TOC/TN-ratios are available due to TN data (TN-values have been below the detection limit). The mean value for TOC/TN is 20.7.

The concentration of $\delta^{13}C_{org}$ is -27.2 ‰ at 90 cm depth and increases to -26.4 ‰ in 180 cm depth. The highest value of -26.2 ‰ is found in 220 cm depth. From 220 to 340 cm the values decrease to -26.7 ‰. The mean value is -26.7 ‰.

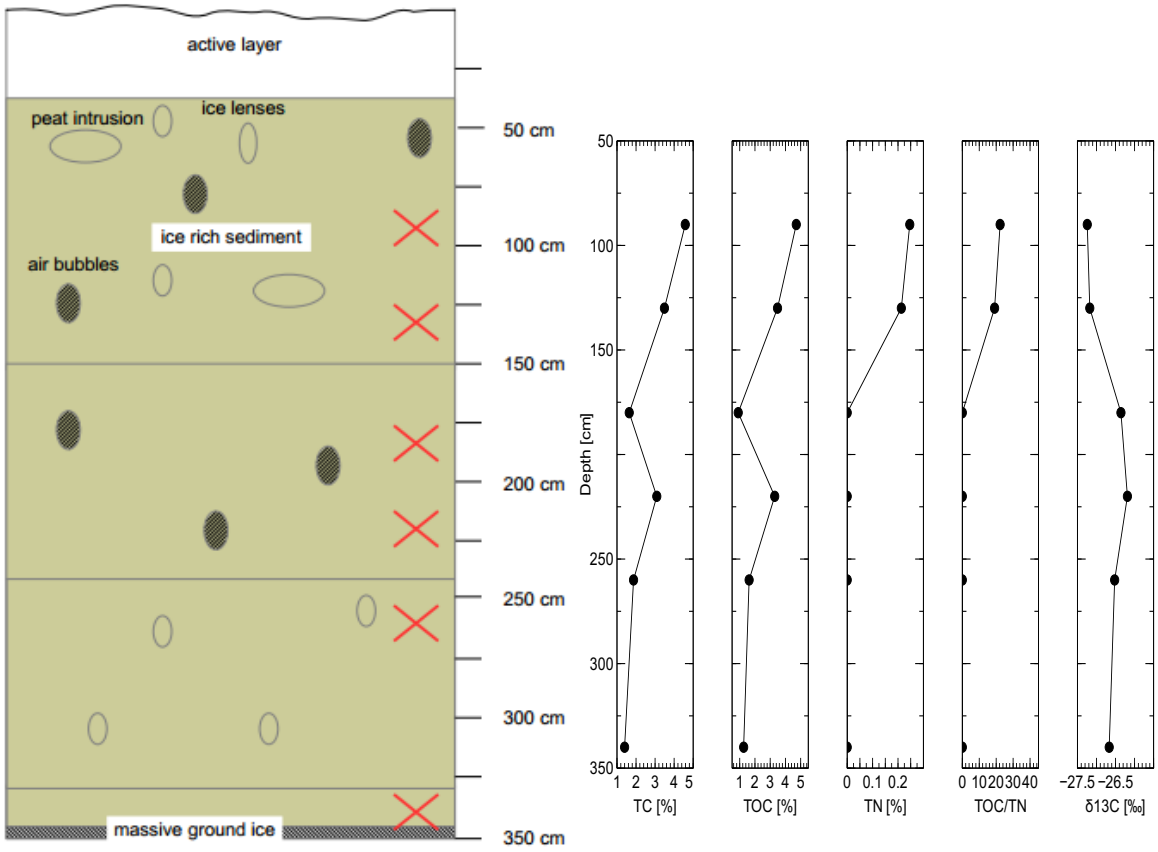

(a) sketch (b) data

Figure 4.5: (a) Sketch: red crosses show sample points, (b) data for permafrost profile 3: summary of biogeochemical and stable isotope parameters. TN and TOC/TN values sink below detection limit and are shown as zero-values.

Table 4.4: Data for permafrost profile 3 along its depth from 90 to 340 cm.

Depth [cm]	TC]%]	TN [%]	TOC/TN	TOC [%]	δ13Corg [‰]
90	4,6	0,2	18,6	4,7	-27,2
130	3,5	0,2	16,4	3,5	-27,2
180	1,6	< 0,10	16,4	0,9	-26,4
220	3,1	< 0,10	30,9	3,3	-26,2
260	1,9	< 0,10	18,7	1,6	-26,5
340	1,4	< 0,10	14,0	1,3	-26,7

To summarise, the highest TC-mean-value is measured for permafrost profile 1, with a mean

value of 10.6 %. Permafrost profile 2 and 3 show rather similar mean values of 2.3 and 2.7 %. TOC-values are the highest in permafrost profile 1 with 10.3 %. For permafrost profile 2 and 3 similar values of 2.1 and 2.5 % are measured. Also TN-values are the highest in permafrost profile 1 with 0.6 %. TN-values of 0.1 and 0.2 % are similar for permafrost profile 2 and 3. The highest mean value for the TOC/TN-ratio shows permafrost profile 3 with 20.7, similar to permafrost profile 2 with 20.1. Lower values are measured for permafrost profile 1 with a mean 19.3 TOC/TN-ratio. $\delta^{13}C_{org}$ are the lowest for permafrost profile 1 with a mean value -27.1 ‰. Permafrost profile 2 and 3 show values of -26.8 and -26.7 %.

4.2 Disturbed zone

4.2.1 Mud pool zone

Samples were taken from the surface (i.e. 0 cm), from 10 cm, and 30 cm depth. The mud pool debris is composed of homogeneous greyish silty clay and is water-saturated. Peat fragments as well as detached hummocks from the tundra can be found throughout the mud pool. Fresh mud pools are free of vegetation. In recently dried out mud pools pioneer vegetation (e.g. grasses) is present and covers up to 40 % of the surface.

Table 4.5: Data for mud pool showing number of samples, range of values, average value and median.

	TC [%] 0cm	TC [%] 10cm	TC [%] 30cm	TOC [%] 0cm	TOC [%] 10cm	TOC [%] 30cm	TN 0cm	TN 10cm	TN 30cm
No. of samples	3	13	14	3	13	14	3	13	14
Range	2.2 - 10.5	1.9 - 4.4	1.9 - 4.2	1.1 - 3.4	0.9 - 2.2	0.7 - 3.5	0.2 - 0.6	<0.1 - 0.3	0.1 - 0.3
Average	5,7	2,5	2,5	2,0	1,2	1,4	0,4	0,2	0,2
Median	4,3	2,3	2,4	1,5	0,2	1,2	0,3	2,0	0,1

	TOC/TN 0cm	TOC/TN 10cm	TOC/TN 30cm	δ13Corg [‰] 0cm	δ13Corg [‰] 10cm	δ13Corg [‰] 30cm
No. of samples	3	13	14	3	13	14
Range	2.0 - 12.8	3.7 - 12.0	3.5 - 12.8	-26.8 - -27.0	-26.6 - -27.1	-26.4 - 27.3
Average	8,5	9,5	10,0	-26,9	-26,9	-26,9
Median	10,7	10,3	10,5	-26,9	-26,9	-27,0

Samples taken from the surface (n = 3) showed TC-values between 2.2 and 10.5 %, with a mean value of 5.7 % (Tab. 4.5). TOC-values range from 1.1 to 3.4 %, with a mean value of 2.0 %. TN-values ranged from 0.2 to 0.6 %, and show a mean value of 0.4 %. The TOC/TN-ratio varies strongly, with values ranging from 2.0 to 12.8, with a mean value of 8.5. Concentrations of $\delta^{13}C_{org}$ range from -27.0 to -26.8 ‰with an mean of -26.9 ‰. Samples taken from 10 cm depth (n = 13) show TC-values of 1.9 to 4.4 %. The mean value is 2.5 %. TOC-values range between 0.9 and 2.2 % with a mean value of 1.2 %. TN-values range from below the detection limit to 0.3 % with a mean value of 0.2 %. The TOC/TN-ratios range from 3.7 to 12.0 with a mean value of 9.5. The $\delta^{13}C_{org}$-values range from -27.1 to -26.6 ‰with a mean value of -26.9 ‰. Samples taken from 30 cm depth (n = 14) have TC-values of 1.9 to 4.2 %, with a mean value of 2.5 %. TOC-values range from 0.7 to 3.5 % with a mean value of 1.4 %. TN-values vary between 0.1 to 0.3 % and show a mean value of 0.2 %. The TOC/TN-ratios range from 3.5 to 12.8 with a mean value of 10.0. The $\delta^{13}C_{org}$-values range between -27.3 and -26.4 ‰with a mean of -26.9 ‰. In conclusion, the mudpool is characterised by low TC-, TOC- and TN-contents. In general TC-, TOC- and TN-values are higher on the surface. Mean TOC/TN-ratios show in all measured depths wide ranges from 3.1 to 12.5. $\delta^{13}C_{org}$-values are similar in all depths with a mean value of -26.9 ‰.

4.2.2 Slump floor zone

The slump floor zone is covered with new and old vegetation. Detached hummocks from the tundra can be found in recently active zones. In general, the slump floor consists of silty-clayey sediments and is covered by mosses and grasses. In parts with steeper slopes and disturbed zones little to no vegetation is present. Slopes can be up to 15°. The vegetation cover differs strongly within the slump and can exceed 80 % surface cover.

Table 4.6: Data for slump floor showing number of samples, range of values, average value and median.

	TC [%] 0cm	TC [%] 10cm	TC [%] 30cm	TOC [%] 0cm	TOC [%] 10cm	TOC [%] 30cm	TN 0cm	TN 10cm	TN 30cm
No. of samples	1	20	19	1	20	19	1	20	19
Range	2,4	1.6 - 21.2	1.8 - 6.5	1,0	0.5 - 7.2	0.7 - 5.0	0,1	0.1 - 1.4	0.1 - 0.5
Average	2,4	4,0	2,7	1,0	1,5	1,2	0,1	0,3	0,2
Median	2,4	2,3	2,2	1,0	1,1	1,0	0,1	0,1	0,1

	TOC/TN 0cm	TOC/TN 10cm	TOC/TN 30cm	δ13Corg [‰] 0cm	δ13Corg [‰] 10cm	δ13Corg [‰] 30cm
No. of samples	1	20	19	1	20	19
Range	8,6	1.5 - 15.9	2.3 - 14.9	-26,8	-25.9 - -27.5	-26.8 - -28.1
Average	8,6	8,7	8,4	-26,8	-27,0	-27,1
Median	8,6	8,9	8,5	-26,8	-27,0	-27,0

One sample (n = 1) has been taken from the surface showing a TC-value of 2.4 %, a TOC-value of 1.0 %, a TN-value of 0.1 % and a TOC/TN-ratio of 8.6. The $\delta^{13}C_{org}$-value is -26.8 ‰ (Tab. 4.6). Samples taken from 10 cm depth (n = 20) show TC-values of 1.6 to 21.2 %, with a mean value of 4.0 %. TOC-values range from 0.5 to 7.2 % with a mean value of 1.5 %. TN-values range from below detection limit of 0.1 % to 1.4 %, with a mean value of 0.3 %. The TOC/TN-ratio ranges from 1.5 to 15.9, with a mean value of 8.7. $\delta^{13}C_{org}$-values range from -27.5 to -25.9 ‰, with a mean of -27.0 ‰. Samples from 30 cm depth (n = 19) show TC-values of 1.8 to 6.5 %, with a mean value of 2.7 %. TOC-values range from 0.7 to 5.0 % with a mean of 1.2 %. TN-values range from 0.1 to 0.5 % with mean of 0.2 %.The TOC/TN-ratio ranges between 2.3 and 14.9, with a mean value of 8.4. $\delta^{13}C_{org}$-values range from -28.1 to -26.8 ‰ with a mean of -27.1 ‰. To sum up, the mean TC-values are the highest at a depth of 10 cm, differing 1.3 % from the values for 30 cm and 1.6 % from the surface sample. Also TOC-values are the highest at a depth of 10 cm, showing differences in mean values of 0.3 % to 30 cm and 0.5 % to the surface sample. The mean TN-values are highest in 10 cm depth, differing by 0.1 % from the samples at a depth of 30 cm and by 0.2 % from the surface sample. The TOC/TN-ratio is very similar between 0, 10 and 30 cm, with a mean value of 8.6. Also $\delta^{13}C_{org}$–values are similar between the depths with around -27.0 ‰.

4.3 Comparison between tundra, permafrost, mud pool and slump floor zone

4.3.1 Comparison of the zones in 10 cm

At 10 cm the tundra zone shows the highest values of TC, TOC and $\delta^{13}C_{org}$ in total, when comparing it to the permafrost, mud pool and slump floor zone. The permafrost zone follows with the next highest values for TC, TOC and $\delta^{13}C_{org}$. The mud pool zone has the lowest values for TC, TOC, followed by the slump floor zone. For $\delta^{13}C_{org}$ the mud pool zone has a slightly higher value than the slump floor zone. TN shows its highest values in the permafrost zone, followed by the tundra, the slump floor and finally the mud pool zone. TOC/TN-ratio is highest in the permafrost zone. The tundra zone shows, next to the permafrost zone, higher values of TOC/TN-ratio than the mud pool and the slump floor zone, whereas the mud pool shows higher values than the slump floor zone.

4.3.2 Comparison of the zones in 30 cm

When comparing the different zones at a depth of 30 cm, the permafrost zone shows throughout all measured parameters the highest values. Looking at TC, the tundra zone shows the next highest values, followed by the slump floor and at last the mud pool zone. For TOC the permafrost zone is followed by the tundra zone, than the mud pool and finally the slump floor zone with lowest values of TOC. When comparing TN-values, the tundra zone has higher values then the mud pool and the slump floor zone, whereas mud pool and slump floor zone show the same mean value. TOC/TN-ratio is, next to the permafrost zone, the highest in the tundra zone, followed by the mud pool and then the slump floor zone. $\delta^{13}C_{org}$ are highest in the permafrost zone, followed by the tundra zone, the mud pool zone and then the slump floor zone, showing the most negative values.

4.3.3 Comparison of the zones in total

All in all it can be said that the tundra zone shows the highest values in TC, TOC, TN and $\delta^{13}C_{org}$. The TC-values for the permafrost zone are the next highest, followed by the mud pool and then the slump floor zone. Same can be said for TOC. The permafrost zone shows,

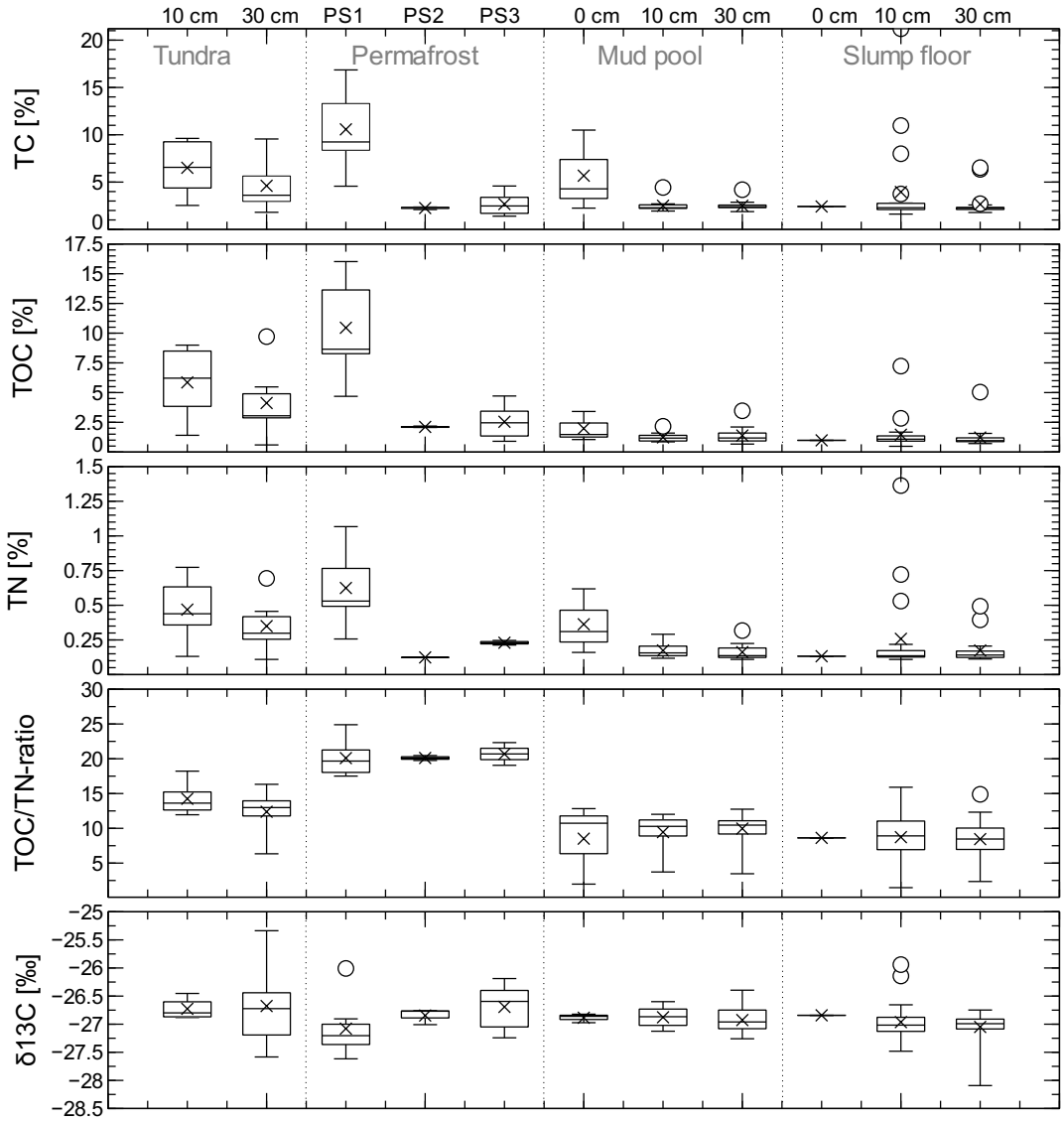

Figure 4.6: Boxplots showing results of biogeochemical and stable isotope parameters for (from left to right) tundra, permafrost profiles, mud pool and slump floor.

next to the tundra zone relatively high TN-values. The slump floor and the mud pool zone show about the same values in TN, but show high differences in the surface samples, where the mud pool shows higher values than the slump floor zone. The highest TOC/TN-values can be seen in the permafrost zone, followed by the tundra zone, the mud pool zone and finally the slump floor zone. $\delta^{13}C_{org}$ is less negative in the tundra zone, and most negative in the mud pool and slump floor zone, where the mud pool zone shows all in all slightly higher (less negative) values than the slump floor zone (Fig. 4.6).

5 Discussion

This chapter compares the TC-, TOC- and TN-values as well as the TOC/TN-ratio and the $\delta^{13}C_{org}$-values for the undisturbed (tundra, permafrost) and disturbed zones (mud pool, slump floor). From the TOC/TN-ratio the origin of the organic material is presented. From the differences in the TOC/TN-ratio and in $\delta^{13}C_{org}$-values the degradation processes are presented.

5.1 TC, TOC and TN quantification in RTS

When comparing the undisturbed zones, tundra and permafrost, with the disturbed zones, mud pool and slump floor, quantitative carbon loss is significant. TC-, TOC- and TN-values are substantially lower in the disturbed zones. Hence permafrost degradation causes losses of carbon and nitrogen. Vegetation cover is a source of carbon and nitrogen, with no plant input on the mud pool and slump floor lower amounts of carbon and nitrogen are available compared to the tundra zone (Traoré et al., 2015). By having a closer look on the correlation of carbon and nitrogen it occurs, that with high TC- and TOC- values high TN-values occur. Which leads to the assumption that carbon dynamics could be affected by nitrogen availability. The disturbed as well as the undisturbed zones show low nitrogen contents, which is usually the case for Arctic soils (Broll et al., 1999; Margesin, 2009).

Kokelj et al. (2002) determined TOC-values of 1.9 to 25.0 % for the uppermost meter on Herschel Island. In comparison, TOC-values of 0.6 to 9.7 % were measured in this study for the uppermost 30 cm in the tundra zone surrounding Slump D. The tundra zone shows, among the analysed zones, highest TC-, TOC- and TN-values. This can be explained by the dense vegetation and the presence of peat and moss, especially in the top layer, where carbon and nitrogen contents are high. However carbon and nitrogen could have been transported into deeper soil layers by cryo- and bioturbation. During cryoturbation some carbon and nitrogen gets released, and some refreezes in deeper depth (U.S., 2003; Bockheim, 2007;

Margesin, 2009). With a warming climate the active layer deepens and thus shows an even higher risk regarding greenhouse gases release due to its high values represented by the tundra zone.

The organic matter of the permafrost origins mainly of litter and root biomass (Couture, 2010). At the top of the permafrost profiles high amounts of TC, TOC and TN compared to greater depths can be found. This is due to cryoturbation and changes in the active layer thickness over time (Schuur et al., 2008). Both processes act as a transfer of OM into deeper depth, where cold temperatures insulates OM for metabolism (Bockheim, 2007; Mueller et al., 2015). Same as in Kokelj et al. (2002) and described by Margesin (2009), in total the permafrost profiles show lower TC-, TOC- and TN-values than the tundra zone, because some labile carbon is already metabolised by microbial activity and cryoturbation while being in the active layer, plus the material is deposited since millennial and in a frozen condition (Tarnocai et al., 2007; Margesin, 2009). Within the permanently frozen sediments microorganisms are mostly inactive so that carbon and nitrogen does not get metabolised (Koven et al., 2009) and is thus not included in the biogeochemical cycles (Winterfeld et al., 2015). It is assumed that the exposed material of permafrost affected areas is more vulnerable to mineralisation because of the climate warming and the induced thawing (Schuur et al., 2008; Harden et al., 2012; Mueller et al., 2015). Different carbon fractions exist that can be decomposed very fast within a few hours to month or slow with turnover rates of a few years up to thousands of years (Parton et al., 1987). With thawing, the more labile carbon and nitrogen release first but the more stable molecules stay in the soil (Schmidt et al., 2011). The more stable molecules can be divided into passive molecules, that stay over hundreds of years in the soil and slow turning over carbon that stays in the soil for several years (Schmidt et al., 2011; Schädel et al., 2014).

The mud pool shows higher TC-, TOC- and TN- values than the slump floor and lower values than the undisturbed zones. Thawing permafrost sediments and plant material from the active layer get mixed in the mud pool. Detached hummocks (peaty blocks of the active layer) get either incorporated and buried in the mud pool or are transported through the gully into the ocean. Areas where gullys form are quite dynamic, thus it is very unlikely for vegetation to grow there. With TOC getting washed into the nearshore zone eutrophication can come along (Krumins et al., 2013).

Dried out areas of the mud pool form and built the slump floor, and show therefore similar low TC-, TOC- and TN-values. Carbon and nitrogen within the mud pool and the slump floor might still get released as greenhouse gases but can also get transported to the nearshore zone

by gullys “draining” the slump. Most labile carbon and nitrogen is already degraded right after thawing before it gets accumulated in the mud pool and slump floor. In the slump floor as well as in the upper part of the mud pool, carbon and nitrogen might be metabolised by microorganisms and released as greenhouse gases into the atmosphere or be preserved in the soil (Koven et al., 2015; MacDougall et al., 2012; Schäfer et al., 2011; Schuur et al., 2013). The organic matter that stays within the soil might stabilise by chemical recalcitrance for several thousands of years (Marschner et al., 2008).The outliers measured in a depth of 10 cm for the mud pool and slump floor zone could be explained by peat lenses or organic remains of already down moved tussocks.

Taking a closer look at the slump floor by comparing the new vegetated zones with the old vegetated zones (Fig. 5.2), the only difference can be seen at 10 cm depth for TC (Fig. 5.2, a)). For a depth of 30 cm (Fig. 5.2, b)), no significant differences can be seen.

(a) new vegetated (b) old vegetated

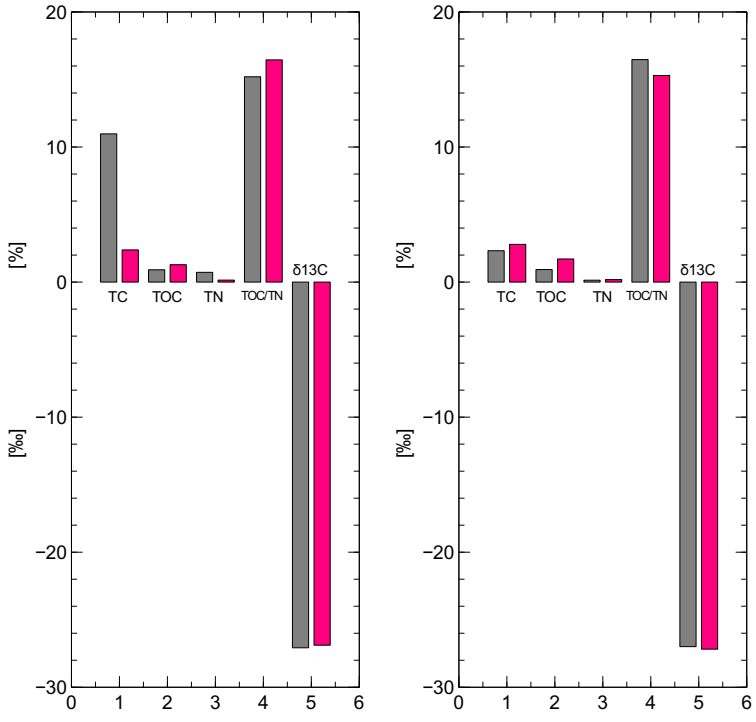

(a) 10 cm (b) 30 cm

Figure 5.2: Slump floor divided into old and new vegetation by an NDVI. Upper Fig. (a) Profile showing new vegetation, (b) profile showing old vegetation; Lower Fig. in grey: new vegetation vs. in pink: old vegetation, comparing biogeochemical and stable isotope parameters, (a) at 10 cm depth, (b) at 30 cm depth.

New vegetated areas within the slump floor show not such high differences to old vegetated areas, because they might not be advanced enough in their stabilisation to show a recovery of the soil yet (Pizano et al., 2014; Cray and Pollard, 2015). With a warmer projected climate plants will grow and might work as carbon sinks. The plants growing on disturbed zones are not to be compared with the vegetation at undisturbed areas, because it differs completely (Lantuit et al., 2012; Cray and Pollard, 2015). Nitrogen released from permafrost might facilitate plant growth. But this process won't compensate degradation and decomposition of carbon and nitrogen from thawing permafrost (Koven et al., 2015).

Next to this study Pizano et al. (2014) came to the conclusion that differences in disturbed and newly undisturbed slumps are detectable. This can also be said for Slump D, where the undisturbed tundra and permafrost zone show higher values of TC, TOC and TN compared to the disturbed mud pool and slump floor zone. To sum up, the tundra zone shows the highest carbon and nitrogen storage and thus implies the highest potential to contribute carbon and nitrogen to the carbon and nitrogen cycle. Organic matter within the mud pool and slump floor zone have been subject to degradation, showing lower carbon and nitrogen amounts. Permafrost stores carbon and nitrogen from the tundra zone, but under frozen conditions, which makes it save for active microorganisms. With its thawing carbon and nitrogen are available for metabolism.

The advantage of using percentage values is typically used because it describes the soil permafrost properties such as potential accumulation and losses. However TC, TOC and TN are dependent on the bulk density of the sediment, so it has to be noticed that their contents in deeper sections of the profiles increase greatly because the density is higher (i.e. Fig. 5.3, for calculation: Appendix). But this does not change the message, that the tundra zone shows the highest TOC and TN values, followed by the mud pool and the slump floor, it rather confirms it.

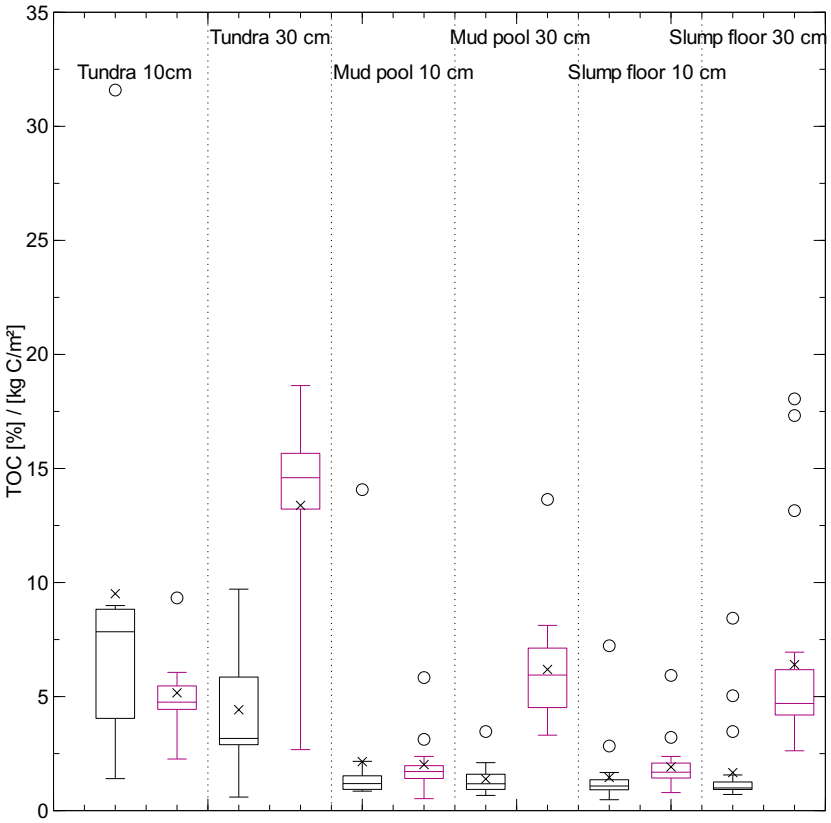

Figure 5.3: Representative for all biogeochemical measured parameters here TOC for (from left to right) tundra, mud pool and slump floor, comparison between: in grey: %, in pink: kg C/m^2.

5.2 Origin of organic material

The calculation of the elemental ratio of TOC/TN together with $\delta^{13}C_{org}$ characterises the sources of organic matter and its environmental conditions during the plant growth period. The origin of organic material depends on the depositional environment that can be either marine, lacustrine or terrestrial (C3 or C4 plants). Low TOC/TN-ratios (4 to 10) and $\delta^{13}C_{org}$-values of -20.0 to -25.0 ‰ are characteristic for marine algae, whereas higher ratios (>20) are characteristic for vascular land plants (Fig. 5.4). If the carbon originates from marine organisms, they are isotopically enriched in $\delta^{13}C_{org}$ because of the uptake of bicarbonate ions (HCO_3^-). With the usage of CO_2, plants take up ^{12}C what makes them depleted in ^{12}C (Lamb et al., 2006). C_3 plants show a higher fractionation associated with CO_2 fixation than the C_4 plants, which use enzyme phosphoenol pyruvate carboxylase (PEP), and thus result in less negative $\delta^{13}C_{org}$-values of -17.0 to -9.0 ‰ (O'Leary et al., 1992; Lamb et al., 2006).

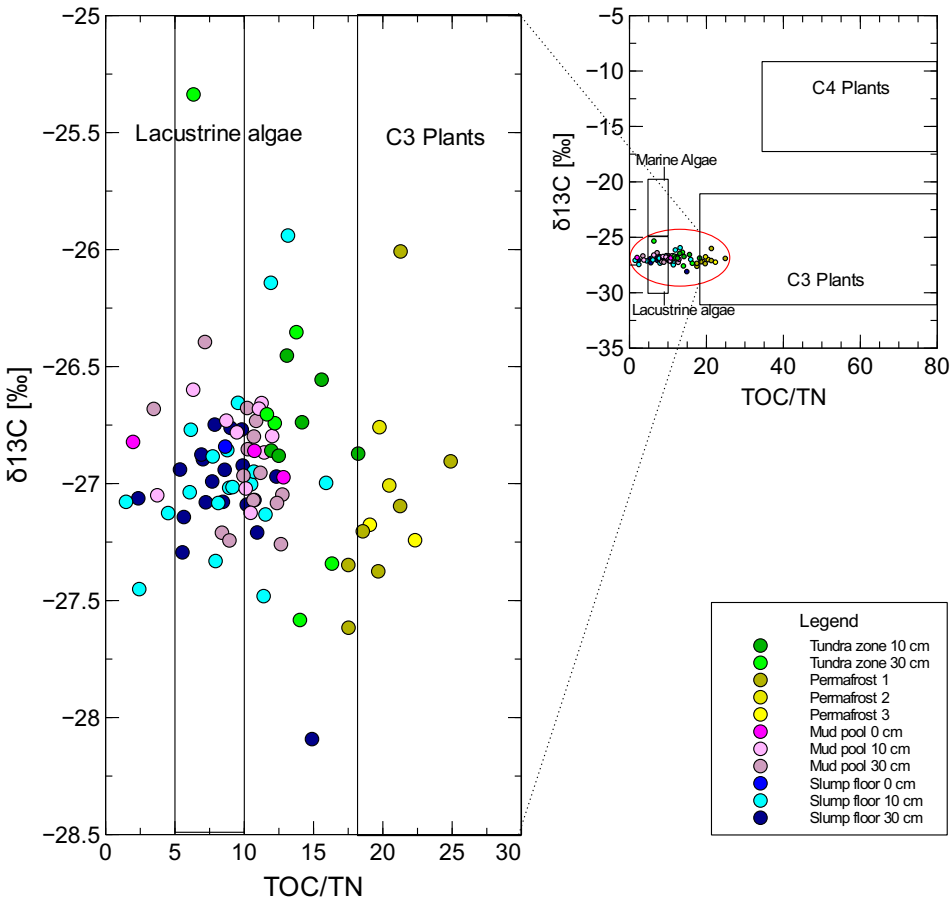

Figure 5.4: Organic carbon source for all measured samples determined by elemental TOC/TN-ratio and isotopic identifiers ($\delta^{13}C_{org}$) (according to Meyers, 1994; Meyers and Lallier-Verges, 1999).

OM from the tundra zone of Slump D originates from lacustrine algae and terrestrial C3-plants with $\delta^{13}C_{org}$-values of -25.3 to -27.6 ‰ and TOC/TN-values of 6.4 to 16.3, whereas OM within the permafrost zone is dominated by terrestrial C3-plants with $\delta^{13}C_{org}$-values of -26.0 to -27.6 ‰ and TOC/TN-values of 14.0 to 30.9 (Fig. 5.4). Tundra as well as permafrost zone show both a mean TOC/TN-ratio of more than 12, indicating that OM originates from terrestrial vegetation, particularly C3 vascular plants, which are depleted in nitrogen (Prahl et al., 1980; Tyson, 1995). OM within the mud pool zone most likely originates from lacustrine algae with $\delta^{13}C_{org}$-values of -26.4 to -27.3 ‰ and TOC/TN-values of 2.0 to 12.8. This is similar and even more evident for the slump floor with $\delta^{13}C_{org}$-values of -25.9 to -28.1 ‰ and TOC/TN-values of 1.5 to 14.9. In total the values range between -25.0 and -29.0 ‰ which is a typical value for the Beaufort Sea region (Naidu et al., 1999). Most of the OM is supposed to be of

marine origin, because Herschel Island consists of marine sediments due to its history of origin (Rampton, 1982; Mackay, 1959). A marine origin is also supported by shell fragments that have been found in the samples. Our TOC/TN data often shows no clear marine or terrestrial signal with a TOC/TN-ratio of 1.5 to 24.8 and $\delta^{13}C_{org}$-values of around -26.8 ‰. A possible explanation is that sediments along the coast are more likely to show a mixture of organic carbon sources, because they get organic material from both autochthonous, and allochthonous sources (Lamb et al., 2006). Also environmental factors, like temperature changes and salinity stress, and decomposition alters $\delta^{13}C_{org}$ and TOC/TN. Especially TOC/TN has to be treated carefully because small changes in TOC or TN can show large changes in the TOC/TN-ratio (Lamb et al., 2006). Bacteria can introduce N in sediments, resulting in a decreased TOC/TN-ratio (Rice and Hanson, 1984). Combined with the presence of algae, determining the organic carbon source can be difficult (Chivas et al., 2001). Rau et al. (1989) show that marine algae in polar sea waters have a $\delta^{13}C_{org}$-value of -28.0 ‰. Fritz (2008) measured same $\delta^{13}C_{org}$-values of -26.3 ‰ and suggests a marine origin of organic matter. Therefore for this study it is suggested that the tundra zone is characterised by terrestrial C3-plants, the permafrost zone represents a mixture of terrestrial C3-plants and marine algae. For the mud pool and slump floor a marine origin is favoured.

5.3 Degradation processes in a RTS system

$\delta^{13}C_{org}$ is used as an indicator for degradation. More negative values result in a low degree of degradation and less negative values result in a high degree of degradation (Strauss et al., 2015). This is due to fractionation processes during metabolism of living plants and during decomposition.

All zones show a $\delta^{13}C_{org}$-value of about -27.0 ‰. No clear difference between the disturbed and undisturbed zones is visible. Comparing the state of degradation by the $\delta^{13}C_{org}$-values with the degree of decomposition by the TOC/TN-ratio a much more obvious signal towards the TOC/TN-ratio is visible. The TOC/TN-ratio is used to determine the degree of OM decomposition. A high TOC/TN-ratio stands for a low degree of decomposition (Schädel et al., 2014; Strauss et al., 2015). Microbial immobilization of TN together with TOC remineralisation and CO_2 emissions result in a low TOC/TN-ratio (Strauss et al., 2015). This is because degradation modifies carbon as well as nitrogen and hence the TOC/TN-ratio. TOC/TN-ratio of lower than 25 ensures microbial activity and thus enables plants to grow. The tundra zone shows higher TOC/TN-ratios than the mud pool and slump floor zone, which indicates a lower degradation

for the tundra compared to the mud pool and slump floor zone. The permafrost zone reflects the stage of decomposition of OM during the freezing processes. It shows the highest values of TOC/TN-ratio and thus indicates a better quality of OM due to the low degraded OM. The low decomposition found for the permafrost zone could be explained by a colder climate and higher vegetation cover during deposition of the material stored in the permafrost (Schuur et al., 2008; Harden et al., 2012). High TOC/TN-ratios represent vulnerable zones, where carbon is available for decomposition (Schädel et al., 2014). Thus, organic matter in permafrost is most likely to degrade rapidly after thawing. The lowest TOC/TN-ratios are measured for the disturbed zones, and thus show a higher degradation and decomposition of the OM than the undisturbed zones. By comparing the TOC/TN-ratios within the permafrost with the mud pool and slump floor it can be said, that carbon and nitrogen get degraded as carbon and nitrogen are very vulnerable to microbial degradation during the thawing of permafrost (Schuur et al., 2008; Schäfer et al., 2011; Harden et al., 2012; Gaglioti et al., 2014). Degradation processes cause a significant reduction of organic carbon and nitrogen (Schädel et al. (2014), Fig. 5.5).

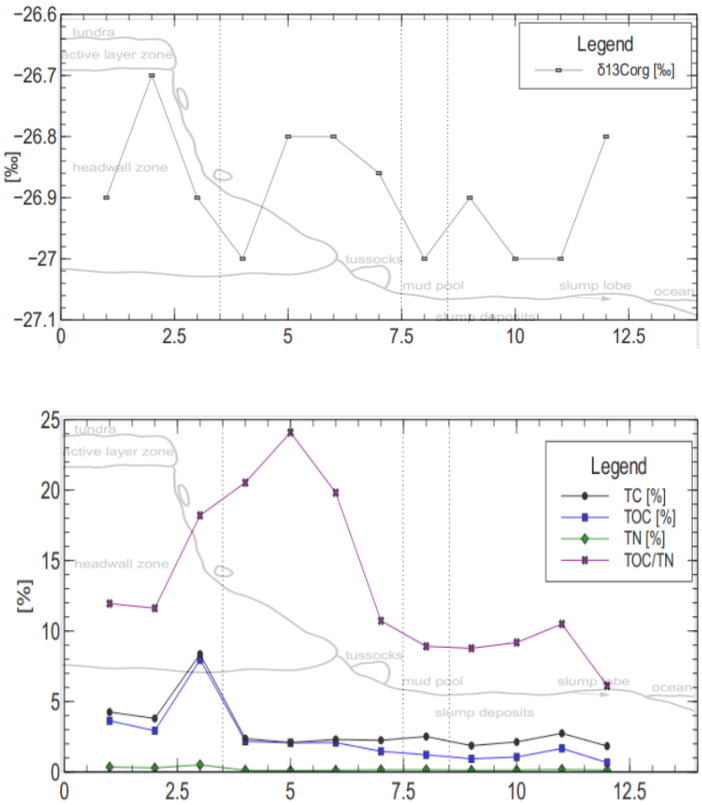

Figure 5.5: Profile through the crosssection of Slump D with overlaid biogeochemical and stable isotope parameters.

The ongoing decomposition within the disturbed zone releases stored carbon into the atmosphere and nitrogen into the soil (Weintraub and Schimel, 2005). This also explains why a low TOC/TN-ratio reflects more degraded zones.

A degradation-depth trend can be seen for the tundra zone. With higher TOC/TN-ratios as well as more negative $\delta^{13}C_{org}$-values in 10 cm the degradation is not that high than in 30 cm. The permafrost zone is less degraded in the upper cm than in the lower cm of the sampled profiles (Fig. 4.3, Fig. 4.4, Fig. 4.5). With the exposed headwall of the slump and a decreasing angle from the headwall to the mud pool, solar radiation can be higher on the shallow, lower part of the headwall, leading to a faster degradation. According to the mean TOC/TN-values the mud pool shows a higher degradation on the surface than in 10 and 30 cm, where in 30 cm depth less degraded material can be found. Less degraded material at 30 cm of the mud pool can be explained by anaerobic conditions found in depth of the mud pool (Schirrmeister et al., 2011). The opposite can be said for the slump floor, showing higher mean TOC/TN-values on the surface and in the upper 10 cm than in 30 cm, and thus a higher degradation in depth. The plants growing on some areas, including old and new vegetation, are responsible for the higher TOC/TN-values on the surface of the slump floor.

6 Conclusion and Outlook

To observe further changes in the degradation processes Slump D and other RTS have to be studied over a long time period. The increasing global air temperature causes permafrost degradation along Arctic coasts that store vast amounts of organic matter. Along the ice-rich Yukon coast, thermokarst and thermoerosional processes have a huge impact on the coastal infrastructure and disturb the coastal landscape. This study shows that during this process organic matter stored in undisturbed tundra and permafrost is subject to significant degradation. Following conclusions can be drawn from this study:

1. Undisturbed coastal zones store with mean values of 4.8 % TOC and 0.4 % TN in the tundra and mean values of 6.7 % TOC and 0.3 % TN in the permafrost zone larger amounts of TOC and TN than disturbed zones with mean values of 1.5 % TOC and 0.3 % TN for the mud pool zone and 1.2 % TOC and 0.2 % TN for the slump floor zone.
2. The organic matter originates from a mixture of lacustrine and terrestrial C3-plants, which can be interpreted as a marine origin for a coastal environment.
3. Organic matter within disturbed zones is highly degraded compared to the undisturbed zones. A degradation towards the coast is visible. The permafrost zone is less degraded than the tundra, mud pool and slump floor, due to its frozen status. High TOC/TN-ratios in the permafrost zone are indicating permafrost as a vulnerable zone, where carbon is available for decomposition (Schäfer et al., 2014). This implicates organic matter in permafrost to be most likely to degrade right after permafrost thaws.
4. No significant differences were determined between old and new vegetated areas within the slump floor.

References

Abbott, B. W., Jones, J. B., 2015. Permafrost collapse alters soil carbon stocks, respiration, ch4, and n2o in upland tundra. Global Change Biology 21 (12), 4570–4587.

Allard, A. M., Pollard, E. W., 2011. Permafrost and climate change in northern coastal canada. Arctic Net, 1–19.

Atkinson, D. E., 2005. Observed storminess patterns and trends in the circum-arctic coastal regime. Geo-Marine Letters 25 (2-3), 98–109.

Bockheim, J., 2007. Importance of cryoturbation in redistributing organic carbon in permafrost/affected soils.

Bouchard, M., 1974. Géologie de dépots de l'ile herschel, territoire du yukon.

Bowden, W., Gooseff, M.N., Balser, A., Green, A., Peterson, B., Bradford, J., 2008. Sediment and nutrient delivery from thermokarst features in the foothills of the north slope, alaska: Potential impacts on headwater stream ecosystems. Journal of Geophysical Research: Biogeosciences (2005–2012) 113 (G2).

Broll, G., Tarnocai, C., Müller, G., 1999. Interactions between vegetation, nutrients and moisture in soild in te pangnirtung pass area, baffin island, canada.

Brown, J., Ferrians, O., Heginbottom, J., Melnikov, E., 1997. International permafrost association, circum-arctic map of permafrost and ground-ice conditions.

Burn, C., 2012. Herschel Island – Qikiqtaryuk, a natural and cultural history of Yukon's Arctic island.

Burn, C., Barrown, E., Bonsal, B., 2004. Climate change scenarios for mackenzie river valley. 57th Canadian Geotechnical Conference,.

Burn, C., Lewkowicz, A., 1990. Canadian landform examples s-17 retrogressive thaw slumps. The Canadian Geographer/Le Géographe canadien 34 (3), 273–276.

Burn, C., Zhang, Y., 2009. Permafrost and climate change at herschel island (qikiqtaruq), yukon territory, canada. Journal of Geophysical Research: Earth Surface (2003–2012) 114 (F2).

Canada, E., 2012. National climate data and information archieve, canadian climate normals 1971-2012.
URL www.climate.weatheroffice.gc.ca

Canadell, J. G., Le Quëré, C., Raupach, M., Field, C., Buitenhuis, E., Ciais, P., Conway, T., Gillett, N., Houghton, R., Marland, G., 2007. Contributions to accelerating atmospheric co2 growth from economic activity, carbon intensity, and efficiency of natural sinks. Proceedings of the national academy of sciences 104 (47), 18866–18870.

Chivas, A. R., Garcia, A., van der Kaars, S., Couapel, M. J., Holt, S., Reeves, J. M., Wheeler, D. J., Switzer, A. D., Murray-Wallace, C. V., Banerjee, D., Price, D. M., Wang, S. X., Pearson, G., Edgar, N., Beaufort, L., Deckker, P. D., Lawson, E., Cecil, C., 2001. Sea-level and environmental changes since the last interglacial in the gulf of carpentaria, australia: an overview. Quaternary International 83–85, 19 – 46.

Couture, N., 2010. Fluxes of soil organic carbon from eroding permafrost coasts, canadian beaufort sea.

Couture, N., Hoque, M., Pollard, W., 2008. Modeling the erosion of ice-rich deposits along the yukon coastal plain. In: Proc. 9 th Int. Permafrost Conference (Alaska). pp. 303–308.

Craig, H., 1953. The geochemistry of the stable carbon isotopes. Geochimica et Cosmochimica Acta 3 (2), 53–92.

Cray, H., Pollard, W., 2015. Vegetation recovery patterns following permafrost disturbance in a low arctic setting: case study of herschel island, yukon, canada. Arctic, Antarctic, and Alpine Research 47 (1), 99–113.

De Krom, V., 1990. Retrogressive thaw slumps and active layer slides on herschel island, yukon.

Douglas, T. A., Fortier, D., Shur, Y. L., Kanevskiy, M. Z., Guo, L., Cai, Y., Bray, M. T., 2011. Biogeochemical and geocryological characteristics of wedge and thermokarst-cave ice in the crrel permafrost tunnel, alaska. Permafrost and Periglacial Processes 22 (2), 120–128.

Fetterer, F., Knowles, K., Meier, W., Savoie, M., 2002. Sea ice index. national snow and ice data center, boulder, co.

Forbes, D., Kremer, H., Lantuit, H., Rachold, V., R.-L., 2011. State of the arctic coast 2010: Scientific review and outlook. International Arctic Science Committee, Land-Ocean Interactions in the Coastal Zone, Arctic Monitoring and Assessment Programme, International Permafrost Association, 1–178.

French, H. M., 2007. The periglacial environment-third edition. John Wiley & Sons.

Fritz, M., 2008. Late quaternary paleoenvironmental records from a glacially and permafrost affected island in the canadian arctic (herschel island, yukon coastal plain).

Fritz, M., Wetterich, S., Meyer, H., Schirrmeister, L., Lantuit, H., Pollard, W. H., 2011. Origin and characteristics of massive ground ice on herschel island (western canadian arctic) as revealed by stable water isotope and hydrochemical signatures. Permafrost and Periglacial Processes 22 (1), 26–38.

Gaglioti, B. V., Mann, D. H., Jones, B. M., Pohlman, J. W., Kunz, M. L., Wooller, M. J., 2014. Radiocarbon age-offsets in an arctic lake reveal the long-term response of permafrost carbon to climate change. Journal of Geophysical Research: Biogeosciences 119 (8), 1630–1651.

Grom, J. D., 2008. Retrogressive thaw slump process and morphology, eureka sound lowlands, ellesmere island, nunavut, canada.

Günther, F., Overduin, P. P., Yakshina, I. A., Opel, T., Baranskaya, A. V., Grigoriev, M. N., 2015. Observing muostakh disappear: permafrost thaw subsidence and erosion of a ground-ice-rich island in response to arctic summer warming and sea ice reduction. The Cryosphere 9 (1), 151–178.

Guo, L., Macdonald, R. W., 2006. Source and transport of terrigenous organic matter in the upper yukon river: Evidence from isotope ($\delta^{13}c$, $\delta^{14}c$, and $\delta^{15}n$) composition of dissolved, colloidal, and particulate phases. Global Biogeochemical Cycles 20 (2).

Handbook, 2005. Handbook Elementar Vario EL III.

Harden, J., Koven, C., Ping, C.-L., Hugelius, G., McGuire, A., Camill, P., Jorgenson, T., Kuhry, P., Michaelson, G., O'Donnell, J., Schuur, E., Tornacai, C., Johnson, K., Grosse, G., 2012. Field information links permafrost carbon to physical vulnerabilities of thawing. Geophysical Research Letters 39 (15).

Harris, S., French, H., Heginbottom, J., Johnston, G., Ladanyi, B., Sego, D., van Everdingen, R.O. Subcommittee, P., 1988. Glossary of permafrost and related ground-ice terms. Associate Committee on Geotechnical Research, National Research Council of Canada, Ottawa, 154.

Heginbottom, J., Brown, J., Humlum, O., S.-H., 2012. Permafrost and periglacial environments.

Hilton, R., Galy, V., Gaillardet, J., Dellinger, M., Bryant, C., O'Regan, M., Gröcke, D., Coxall, H., Bouchez, J., Calmels, D., 2015. Erosion of organic carbon in the arctic as a geological carbon dioxide sink. Nature 524.

Hugelius, G., Strauss, J., Zubrzycki, S., Harden, J., Schuur, E., Ping, C., Schirrmeister, L., Gosse, G., Michaelson, G., Koven, C., O'Donnell, J., Elberling, B., Mishra, U., Camill, P., Yu, Z., Palmtag, J., Kuhry, P., December 2014. Estimated stocks of circumpolar permafrost carbon with quantified uncertainty ranges and identified data gaps. Biogeosciences 11 (23), 6573–6593.

Jorgenson, M., Racine, C., Walters, J., Osterkamp, T., 2001. Permafrost degradation and ecological changes associated with a warmingclimate in central alaska. Climatic Change 48 (4), 551–579.

Kanevskiy, M., Shur, Y., Jorgenson, M., Ping, C.-L., Michaelson, G., Fortier, D., Stephani, E., Dillon, M., Tumskoy, V., 2013. Ground ice in the upper permafrost of the beaufort sea coast of alaska. Cold Regions Science and Technology 85, 56 – 70.

Kennedy, C., 2012. Herschel island qikiqtaryuk: A natural and cultural history of yukon's arctic island (edited by christopher r. burn).

Kokelj, A., Lewkowicz, A. G., 1999. Salinization of permafrost terrain due to natural geomorphic disturbance, fosheim peninsula, ellesmere island. Arctic, 372–385.

Kokelj, S., Lacelle, D., Lantz, T., Tunnicliffe, J., Malone, L., Clark, I., Chin, K., 2013. Thawing of massive ground ice in mega slumps drives increases in stream sediment and solute

flux across a range of watershed scales. Journal of Geophysical Research: Earth Surface 118 (2), 681–692.

Kokelj, S., Lntz, T., Kanigan, J., Smith, S., Coutts, R., 2009. Origin and polycyclic behaviour of tundra thaw slumps, mackenzie delta region, northwest territories, canada. Permafrost and Periglacial Processes 20 (2), 173–184.

Kokelj, S., Pisaric, M., Burn, C., 2002. Physical and chemical characteristics of the active layer and permafrost, herschel island, western arctic coast, canada. Permafrost and Periglacial Processes 13 (2), 171–185.

Kokelj, S., Tunnicliffe, J., Lacelle, D., Lantz, T., Chin, K., Fraser, R., 2015. Increased precipitation drives mega slump development and destabilization of ice-rich permafrost terrain, northwestern canada. Global and Planetary Change 129, 1–53.

Kokelj, S. V., Jorgenson, M. T., 2013. Advances in thermokarst research. Permafrost and Periglacial Processes 24 (2), 108–119.

Koven, C., Friedlingstein, P., Ciais, P., Khvorostyanov, D., Krinner, G., Tarnocai, C., 2009. On the formation of high-latitude soil carbon stocks: effects of cryoturbation and insulation by organic matter in a land surface model. Geophysical Research Letters 36, L21501.

Koven, C. D., Lawrence, D. M., Riley, W. J., 2015. Permafrost carbon- climate feedback is sensitive to deep soil carbon decomposability but not deep soil nitrogen dynamics. Proceedings of the National Academy of Sciences 112 (12), 3752–3757.

Krumins, V., Gehlen, M., Arndt, S., Van Cappellen, P., Regnier, P., 2013. Dissolved inorganic carbon and alkalinity fluxes from coastal marine sediments: model estimates for different shelf environments and sensitivity to global change. Biogeosciences 10 (1), 371–398.

Lacelle, D., Bjornson, J., Lauriol, B., 2010. Climatic and geomorphic factors affecting contemporary (1950–2004) activity of retrogressive thaw slumps on the aklavik plateau, richardson mountains, nwt, canada. Permafrost and Periglacial Processes 21 (1), 1–15.

Lamb, A. L., Wilson, G. P., Leng, M. J., 2006. A review of coastal palaeoclimate and relative sea-level reconstructions using δ 13 c and c/n ratios in organic material. Earth-Science Reviews 75 (1), 29–57.

Lantuit, H., Atkinson, D., Overduin, P. P., Grigoriev, M., Rachold, V., Grosse, G., Hubberten, H.-W., 2011. Coastal erosion dynamics on the permafrost-dominated bykovsky peninsula, north siberia, 1951-2006. Polar Research 30.

Lantuit, H., Overduin, P., Couture, N., Wetterich, S., Aré, F., Atkinson, D., Brown, J., Cherkashov, G., Drozdov, D., Forbes, D., Graves-Gaylord, A., Grigoriev, M., Hubberten, H.-W., Jordan, J., Jorgenson, T., Ødegård, R. S., Ogorodov, S., Pollard, W. H., Rachold, V., Sedenko, S., Solomon, S., Steenhuisen, F., Streletskaya, I., Vasiliev, A., 2012a. The arctic coastal dynamics database: A new classification scheme and statistics on arctic permafrost coastlines. Estuaries and Coasts 35 (2), 383–400.

Lantuit, H., Pollard, W., 2005. Temporal stereophotogrammetric analysis of retrogressive thaw slumps on herschel island, yukon territory. Natural Hazards and Earth System Science 5 (3), 413–423.

Lantuit, H., Pollard, W., 2008. Fifty years of coastal erosion and retrogressive thaw slump activity on herschel island, southern beaufort sea, yukon territory, canada. Geomorphology 95 (1), 84–102.

Lantuit, H., Pollard, W., Couture, N., Fritz, M., Schirrmeister, L., Meyer, H., Hubberten, H.-W., 2012. Modern and late holocene retrogressie thaw slump activity on the yukon coastal plain and herschel islnd, yukon territory, canada. Permafrost and Periglacial Processes 23 (1), 39–51.

Lantuit, H., Schirrmeister, L., 2012b. Permafrost und mensch (permafrost and man). Polarforschung 81 (1), 69–75.

Larouche, J., Abbott, B., Bowden, W., Jones, J., 2015. The role of watershed characteristics, permafrost thaw, and wildfire on dissolved organic carbon biodegradability and water chemistry in arctic headwater streams. Biogeosciences Discussions 12 (5), 4021–4056.

Lawrence, D. M., Slater, A. G., 2005. A projection of severe near-surface permafrost degradation during the 21st century. Geophysical Research Letters 32 (24).

Lawrence, D. M., Slater, A. G., Swenson, S., 2011. Simulation of present-day and future permafrost and seasonally frozen ground conditions in ccsm4. J Clim.

MacDougall, A. H., Avis, C. A., Weaver, A. J., 2012. Significant contribution to climate warming from the permafrost carbon feedback. Nature Geoscience 5 (10), 719–721.

Mackay, J., 1972. The world of underground ice. Annals of the Association of American Geographers 62 (1), 1–22.

Mackay, J. R., 1959. Glacier ice-thrust features of the yukon coast. Geographical Bulletin 13, 5–21.

Mackay, J. R., 1989. Massive ice: some field criteria for the identification of ice types. Current Research, Part G, Geological Survey of Canada, Paper, 5–11.

Margesin, R., 2009. Soil biology - permafrost soils. Springer Verlag Berlin, 3–16.

Marschner, B., Brodowski, S., Dreves, A., Gleixner, G., Gude, A., Grootes, P. M., Hamer, U., Heim, A., Jandl, G., Ji, R., Kaiser, K., Kalbitz, K., Kramer, C., Leinweber, P., Rethemeyer, J., Schäffer, A., Schmidt, M. W. I., Schwark, L., Wiesenberg, G. L. B., 2008. How relevant is recalcitrance for the stabilization of organic matter in soils? Journal of Plant Nutrition and Soil Science 171 (1), 91–110.

Meyers, P., 1994. Preservation of elemental and isotopic source identification of sedimentary organic matter. Chemical Geology 114 (3), 289–302.

Meyers, P., Lallier-Verges, E., 1999. Lacustrine sedimentary organic matter records of late quaternary paleoclimates. Journal of Paleolimnology 21 (3).

Muccio, Z., Jackson, G. P., 2009. Isotope ratio mass spectrometry. Analyst 134 (2), 213–222.

Mueller, C. W., Rethemeyer, J., Kao-Kniffin, J., Löppmann, S., Hinkel, K. M., Bockheim, J. G., 2015. Large amounts of labile organic carbon in permafrost soils of northern alaska. Global change biology 21.

Myers-Smith, I., Hik, D., Kennedy, C., Cooley, C., Johnstone, J., Kennedy, A., Krebs, C., 2011. Expansion of canopy-forming willows over the twentieth century on herschel island, yukon territory, canada. Ambio 40 (6), 610–623.

Naidu, A., Cooper, L., Finney, B., MacDonald, R., Alexander, C., Semiletov, I., 1999. Organic carbon isotope ratios $\delta^{13}c$ of arctic amerasian continental shelf sediments. Int. J. Earth Sciences 89.

Obu, J., Lantuit, H., Myers-Smith, I., Heim, B., Wolter, J., Fritz, M., 2015. Effect of terrain on soil organic carbon and total nitrogen in soils of herschel island, western canadian arctic. Permafrost and Periglacial Processes Journal.

O'Leary, M., Madhavan, S., Paneth, P., 1992. Physical and chemical basis of carbon isotope fractionation in plants. Plant, Cell and Environment 15, 1099–1104.

Oserkamp, T., Jorgenson, M., Schuur, E., Shur, Y., Kanevskiy, M., Vogel, J., Tumskoy, V., 2009. Physical and ecological changes associated with warming permafrost and thermokarst in interior alaska. Climatic change 20.

Pachauri, R. K., Allen, M., Barros, V., Broome, J., Cramer, W., Christ, R., Church, J., Clarke, L., Dahe, Q., Dasgupta, P., et al., 2014. Climate change 2014: Synthesis report. contribution of working groups i, ii and iii to the fifth assessment report of the intergovernmental panel on climate change.

Parton, W., Schimel, D., Cole, C., Ojima, D., 1987. Analysis of factors controlling soil organic matter levels in great plains grasslands. Soil Science Society of America Journal 51 (5), 1173–1179.

Pizano, C., Barón, A., Schuur, E., Crummer, K., Mack, M., 2014. Effects of thermo-erosional disturbance on surface soil carbon and nitrogen dynamics in upland arctic tundra. Environmental Research Letters 9 (7), 1–13.

Pollard, W., 1990. The nature and origin of ground ice in the herschel island area, yukon territory, 23–30.

Prahl, F., Bennett, J., Carpenter, R., 1980. The early diagenesis of aliphatic hydrocarbons and organic matter in sedimentary particulates from dabob bay, washington. Geochimica et Cosmochimica Acta 44 (12), 1967 – 1976.

Rachold, V., Aré, F., Atkinson, D., Cherkashov, G., Solomon, S., 2005. Arctic coastal dynamics (acd): an introduction. Geo-Marine Letters 25 (2-3), 63–68.

Radosavljevic, B., Lantuit, H., Pollard, W., Overduin, P., Couture, N., Sachs, T., Helm, V., Fritz, M., 2015. Erosion and flooding—threats to coastal infrastructure in the arctic: A case study from herschel island, yukon territory, canada. Estuaries and Coasts, 1–16.

Rampton, V., 1982. Quaternary geology of the yukon coastal plain. Bulletin Geological Survey of Canada 317, 1–49.

Rau, G., Takahashi, T., Des Marais, D., 1989. Latitudinal variations in plankton c: implications for co and productivity in past oceans. Nature 341 (5), 165.

Rice, D. L., Hanson, R. B., 1984. A kinetic model for detritus nitrogen: Role of the associated bacteria in nitrogen accumulation. Bulletin of Marine Science 35 (3), 326–340.

Robinson, S., 2000. Thaw slump derived thermokarst near hot weather creek, ellesmere island, nunavut. Bulletin Geological Survey of Canada 529, 335–345.

Romanovsky, V., Gruber, S., Instanes, A., Jin, H., Marchenko, S., Smith, S., Trombotto, D., Walter, K., 2007. Frozen ground.

Romanovsky, V., Smith, S., Christiansen, H., 2010. Permafrost thermal state in the polar northern hemisphere during the international polar year 2007–2009: a synthesis. Permafrost and Periglacial Processes 21 (2), 106–116.

Rothrock, D. A., Zhang, J., 2005. Arctic ocean sea ice volume: What explains its recent depletion? Journal of Geophysical Research: Oceans 110 (C1), n/a–n/a, c01002.

Saito, K., Kimoto, M., Zhang, T., Takata, K., Emori, S., 2007. Evaluating a high-resolution climate model: Simulated hydrothermal regimes in frozen ground regions and their change under the global warming scenario. Journal of Geophysical Research: Earth Surface 112 (F2).

Schädel, C., Schuur, E., Bracho, R., Elberling, B., Knoblauch, C., Lee, H., Luo, Y., Shaver, G., Turetsky, M., 2014. Circumpolar assessment of permafrost c quality and its vulnerability over time using long-term incubation data. Global Change Biology 20 (2), 641–652.

Schäfer, K., Lantuit, H., Romanovsky, V. E., Schuur, E., Witt, R., 2014. The impact of the permafrost carbon feedback on global climate. Environmental Research Letters 9 (8), 085003.

Schäfer, K., Zhang, T., Bruhwiler, L., Barrett, A., 2011. Amount and timing of permafrost carbon release in response to climate warming. Tellus B 63 (2), 165–180.

Schirrmeister, L., Kunitsky, V., Grosse, G., Wetterich, S., Meyer, H., Schwamborn, G., Babiy, O., Derevyagin, A., Siegert, C., 2011. Sedimentary characteristics and origin of the late pleistocene ice complex on north-east siberian arctic coastal lowlands and islands – a review. Quaternary International 241 (1–2), 3 – 25.

Schmidt, M., Torn, M., Abiven, S., Dittmar, T., Guggenberger, G., Janssens, I. A., Kleber, M., Kögel-Knabner, I., Lehmann, J., Manning, D., et al., 2011. Persistence of soil organic matter as an ecosystem property. Nature 478 (7367), 49–56.

Schuur, E., Abbott, B., Koven, C., Riley, W., Subin, Z., 2013. High risk of permafrost thaw. Nature, 2011.

Schuur, E., Bockheim, J., Canadell, J., Euskirchen, E., Field, C., Goryachkin, S., Hagemann, S., Kuhry, P., Lafleur, P., Lee, H., Mazhitova, G., Nelson, F., Rinke, A., Romanovsky, V., Shiklomanov, N., Tarnocai, C., Venevsky, S., Vogel, J., Zimov, S., 2008. Vulnerability of permafrost carbon to climate change: Implications for the global carbon cycle. BioScience 58 (8), 701–714.

Schuur, E., McGuire, A., Schädel, C., Grosse, G., Harden, J., Hayes, D., Hugelius, G., Koven, C., Kuhry, P., Lawrence, D., Natali, S., Olefedt, D., Romanovsky, V., Schäfer, K., Turetsky, M., Treat, C., Vonk, J., 2015. Climate change and the permafrost carbon feedback. Nature.

Schuur, E., Vogel, J., Crummer, K., Lee, H., Sickman, J., Osterkamp, T., 2009. The effect of permafrost thaw on old carbon release and net carbon exchange from tundra. Nature.

Serreze, M., Francis, J., 2006. The arctic amplification debate. Climatic Change 76 (3-4), 241–264.

Serreze, M., Stroeve, J., 2015. Arctic sea ice trends, variability and implications for seasonal ice forecasting. Philosophical Transactions of the Royal Society of London A: Mathematical, Physical and Engineering Sciences 373 (2045).

Shumskii, P., 1959. Ground (subsurface) ice.

Sloan, H., Pollard, W., 2012. Vegetation patterns of stabilized retrogressive thaw slumps, herschel island, northern yukon. Proceedings of the Tenth International Conference on Permafrost, 389–393.

Smith, S., Burgess, M., 2000. Ground temperature database for northern Canada. Geological Survey of Canada.

Smith, S., Burgess, M., 2004. Sensitivity of permafrost to climate warming in Canada. Geological Survey of Canada.

Smith, S., Burgess, M., Heginbottom, J., 2001. Permafrost in canada, a challenge to northern development. A synthesis of geological hazards in Canada. Geological Survey of Canada, Bulletin 548, 241–264.

Smith, S., Burgess, M., Riseborough, D., Nixon, F., 2005. Recent trends from canadian permafrost thermal monitoring network sites. Permafrost and Periglacial Processes 16 (1), 19–30.

Solomon, S. M., 2005. Spatial and temporal variability of shoreline change in the beaufort-mackenzie region, northwest territories, canada. Geo-Marine Letters 25 (2-3), 127–137.

Strauss, J., Schirrmeister, L., Grosse, G., Wetterich, S., Ulrich, M., Herzschuh, U., Hubberten, H.-W., 2013. The deep permafrost carbon pool of the yedoma region in siberia and alaska. Geophysical Research Letters 40 (23), 6165–6170.

Strauss, J., Schirrmeister, L., Mangelsdorf, K., Eichhorn, L., Wetterich, S., Herzschuh, U., 2015. Organic-matter quality of deep permafrost carbon-a study from arctic siberia. Biogeosciences 12 (7), 2227–2245.

Stroeve, J., Kattsov, V., Barrett, A., Serreze, M., Pavlova, T., Holland, M., Meier, W., 2012. Trends in arctic sea ice extent from cmip5, cmip3 and observations. Geophys. Res. Lett. 39.

Sundquist, E., Visser, K., 2004. Biogeochemistry 8.

Tanski, G., 2013. Release of dissolved organic carbon from coastal erosion into the southern canadian beaufort sea.

Tarnocai, C., Canadell, J., Schuur, E., Kuhry, P., Mazhitova, G., Zimov, S., 2009. Soil organic carbon pools in the northern circumpolar permafrost region. Global Biogeochemical Cycles 23 (2), GB2023.

Tarnocai, C., Ping, C., Kimble, J., King, A., Dilling, L., Zimmerman, G., Fairman, D., Houghton, R., Marland, G., Rose, A., et al., 2007. Carbon cycles in the permafrost region of north america. The First State of the Carbon Cycle Report (SOCCR): The North American Carbon Budget and Implications for the Global Carbon Cycle. A report by the US, 127–138.

Tarnocai, C., Stolbovoy, V., 2006. Northern peatlands: Their characteristics, development and sensitivity to climate change 9.

Traoré, S., Ouattara, K., Ilstedt, U., Schmidt, M., Thiombiano, A., Malmer, A., Nyberg, G., 2015. Effect of land degradation on carbon and nitrogen pools in two soil types of a semi-arid landscape in west africa. Geoderma 241–242, 330 – 338.

Tyson, R., 1995. Sedimentary organic matter: organic facies and palynofacieschapman and hall. London, New York.

U.S., 2003. U.s. arctic research commission permafrost task force. climate change, permafrost, and impacts on civil infrastructure.

Van Everdingen, R., 2005. Mulit-language glossary of permafrost and related ground-ice terms.

Von Lozinski, W., 1909. Über die mechanische verwitterung der sandsteine im gemässigten klima. Bulletin international de l'Academie des Sciences de Cracovie. Classe des Sciences athematques et Naturelles 1, 1//25.

Walsh, J., Overland, J., Groisman, P., Rudolf, B., 2011. Ongoing climate change in the arctic. Ambio 40, 6–16.

Weintraub, M., Schimel, J., 2003. Interactions between carbon and nitrogen mineralization and soil organic matter chemistry in arctic tundra soils. Ecosystems 6 (2), 129–143.

Weintraub, M., Schimel, J., 2005. Nitrogen cycling and the spread of shrubs control changes in the carbon balance of arctic tundra ecosystems. BioScience 55 (5), 408–415.

Winterfeld, M., Goni, M., Just, J., Hefter, J., Mollenhauer, G., 2015. Characterization of particulate organic matter in the lena river delta and adjacent nearshore zone, ne siberia-part2: Lignin-derived phenol compositions. Biogeosciences 12, 2261–2283.

Wolfe, S., Kotler, E., Nixon, M., 2000. Recent warming impacts in the mackenzie delta, northwest territories, and northern yukon territory coastal areas. current research 2000-b1, geological survey of canada. Natural Resources Canada, Ottawa 9.

Woo, M.-K., Ohmura, A., 1997. The arctic islands. The Surface Climates of Canada. Canadian Association of Geographers Series in Canadian Geography 4, 172–197.

Wood, K., Bond, N., Danielson, S., Overland, J., Salo, S., Stabeno, P., Whitefield, J., 2015. A decade of environmental change in the pacific arctic region. Progress in Oceanography 136, 12 – 31, synthesis of Arctic Research (SOAR).

Zimov, S., Davydov, S., Zimova, G., Davydova, A., Schuur, E., Dutta, K., Chapin III, F., 2006. Permafrost carbon: Stock and decomposability of a globally significant carbon pool. Geophysical Research Letters 33 (20), L20502.

Appendix

Zone	Zone	Sample_ID	Depth [cm]	Latitude	Longitude	Wet weight	Dry weight	Volume	TC	TN	C/N-ratio	TOC	d13C	Volume (cm3)	BD	SOC (Kg C/m2)
Tundra	1	SlpD14-TS-F14-01	10	69,571383	-139,014576	288,30	213,61	211,82	4,76	0,37	12,97	4,45	-26,74	211,80	1,01	4,49
Tundra	1	SlpD14-TS-H14-01	10	69,571581	-139,017533	347,37	277,10	211,82	4,25	0,35	11,98	3,64	-26,86	211,80	1,31	4,76
Tundra	1	SlpD14-TS-N14-01	10	69,569810	-139,020331	228,29	107,20	211,82	9,56	0,77	12,36	8,67	-26,45	211,80	0,51	4,39
Tundra	1	SlpD14-TS-P13-01	10	69,568914	-139,020414	228,27	142,79	211,82	9,62	0,67	14,28	8,99	-26,56	211,80	0,67	6,06
Tundra	1	SlpD14-TS-R10-01	10	69,567093	-139,018016	404,15	341,28	211,82	2,53	0,13	19,31	1,40	-26,88	211,80	1,61	2,26
Tundra	1	SlpD14-TS-PS2-01	10	69,571333	-139,016618	607,66	179,28	211,82	8,36	0,51	16,38	7,97	-26,87	211,80	0,00	0,00
Zone	Zone	Sample_ID	Depth [cm]	Latitude	Longitude	Wet weight	Dry weight	Volume	TC	TN	C/N-ratio	TOC	d13C	Volume (cm3)	BD	SOC (Kg C/m2)
Tundra	1	SlpD14-TS-F14-02	30	69,571383	-139,014576	403,36	325,50	211,82	3,42	0,30	11,30	3,17	-26,74	211,80	1,54	14,60
Tundra	1	SlpD14-TS-H14-02	30	69,571581	-139,017533	382,54	314,43	211,82	3,80	0,29	12,94	2,93	-26,70	211,80	1,48	13,04
Tundra	1	SlpD14-TS-J15-02	30	69,571135	-139,018869	255,98	117,73	211,82	9,56	0,69	13,77	9,71	-27,34	211,80	0,56	16,19
Tundra	1	SlpD14-TS-N14-02	30	69,569810	-139,020331	473,34	331,23	211,82	2,81	0,24	11,58	2,86	-26,35	211,80	1,56	13,40
Tundra	1	SlpD14-TS-P13-02	30	69,568914	-139,020414	351,14	240,18	211,82	6,26	0,46	13,72	5,48	-27,58	211,80	1,13	18,64
Tundra	1	SlpD14-TS-R10-02	30	69,567093	-139,018016	398,78	317,50	211,82	1,81	0,11	16,52	0,59	-25,34	211,80	1,50	2,68

Zone	Zone	Sample_ID	Depth [cm]	Latitude	Longitude	Wet weight	Dry weight	Volume	TC	TN	C/N-ratio	TOC	d13C
Ice Exposure	2	SlpD14-TS-PS1-01	40	69,571219	-139,016257	483,33	173,87	211,82	16,85	1,07	15,79	16,02	-27,62
Ice Exposure	2	SlpD14-TS-PS1-02	90	69,571219	-139,016257	211,33	76,82	211,82	8,36	0,53	15,77	7,95	-27,35
Ice Exposure	2	SlpD14-TS-PS1-03	120	69,571219	-139,016257	361,36	147,20	211,82	8,37	0,51	16,31	8,65	-27,38
Ice Exposure	2	SlpD14-TS-PS1-04	150	69,571219	-139,016257	305,05	95,94	211,82	15,99	0,99	16,09	15,80	-27,20
Ice Exposure	2	SlpD14-TS-PS1-05	190	69,571219	-139,016257	351,27	143,62	211,82	9,24	0,47	19,58	8,59	-27,10
Ice Exposure	2	SlpD14-TS-PS1-06	220	69,571219	-139,016257	344,74	153,91	211,82	10,61	0,54	19,74	11,47	-26,91
Ice Exposure	2	SlpD14-TS-PS1-07	250	69,571219	-139,016257	355,27	154,79	211,82	4,57	0,26	17,77	4,68	-26,01
Zone	Zone	Sample_ID	Depth [cm]	Latitude	Longitude	Wet weight	Dry weight	Volume	TC	TN	C/N-ratio	TOC	d13C
Ice Exposure	2	SlpD14-TS-PS2-02	100	69,571333	-139,016618	349,52	219,17	211,82	2,37	0,12	19,02	2,18	-27,01
Ice Exposure	2	SlpD14-TS-PS2-03	150	69,571333	-139,016618	570,11	273,87	211,82	2,10	< 0,10	20,98	2,06	-26,77
Ice Exposure	2	SlpD14-TS-PS2-04	190	69,571333	-139,016618	241,52	103,56	211,82	2,31	0,12	18,72	2,09	-26,76
Zone	Zone	Sample_ID	Depth [cm]	Latitude	Longitude	Wet weight	Dry weight	Volume	TC	TN	C/N-ratio	TOC	d13C
Ice Exposure	2	SlpD14-TS-PS3-01	90	69,571152	-139,012364	384,50	131,03	211,82	4,58	0,25	18,61	4,71	-27,24
Ice Exposure	2	SlpD14-TS-PS3-02	130	69,571152	-139,012364	398,06	141,66	211,82	3,49	0,21	16,38	3,48	-27,18
Ice Exposure	2	SlpD14-TS-PS3-03	180	69,571152	-139,012364	356,24	263,02	211,82	1,64	< 0,10	16,43	0,90	-26,36
Ice Exposure	2	SlpD14-TS-PS3-04	220	69,571152	-139,012364	563,96	338,14	211,82	3,09	< 0,10	30,89	3,30	-26,19
Ice Exposure	2	SlpD14-TS-PS3-05	260	69,571152	-139,012364	608,98	391,18	211,82	1,87	< 0,10	18,69	1,62	-26,52
Ice Exposure	2	SlpD14-TS-PS3-06	340	69,571152	-139,012364	417,59	287,85	211,82	1,40	< 0,10	13,99	1,26	-26,67

Zone	Zone	Sample_ID	Depth [cm]	Latitude	Longitude	Wet weight	Dry weight	Volume	TC	TN	C/N-ratio	TOC	d13C	Volume (cm3)	BD	SOC (Kg C/m2)
Mud Pool	3	SlpD14-TS-F13-01	6	69,571082	-139,013793	275,11	158,99	211,82	4,29	0,31	13,82	3,41	-26,97	211,80	0,75	1,54
Mud Pool	3	SlpD14-TS-H13-01	6	69,571111	-139,016358	392,02	303,65	211,82	2,25	0,16	14,06	1,47	-26,86	211,80	1,43	1,27
Mud pool	3	SlpD14-TS-J14-01	6	69,570677	-139,017683	380,36	289,75	211,82	10,49	0,62	16,97	1,05	-26,82	211,80	1,37	0,86
Zone	Zone	Sample_ID	Depth [cm]	Latitude	Longitude	Wet weight	Dry weight	Volume	TC	TN	C/N-ratio	TOC	d13C	Volume (cm3)	BD	SOC (Kg C/m2)
Mud Pool	3	SlpD14-TS-F10-01	10	69,570157	-139,011311	368,32	306,10	211,82	2,54	0,22	11,31	2,16	-26,66	211,80	1,45	3,12
Mud Pool	3	SlpD14-TS-F11-01	10	69,570619	-139,012552	350,96	266,76	211,82	2,60	0,21	12,17	1,59	-26,73	211,80	1,26	2,00
Mud Pool	3	SlpD14-TS-F12-01	10	69,570619	-139,012552	411,30	332,75	211,82	2,24	0,14	15,56	1,17	-26,78	211,80	1,57	1,84
Mud Pool	3	SlpD14-TS-F9-01	10	69,569694	-139,010070	385,29	320,94	211,82	2,44	0,18	13,48	1,57	-27,02	211,80	1,52	2,38
Mud Pool	3	SlpD14-TS-H12-01	10	69,570648	-139,015117	219,55	87,81	211,82	12,57	0,75	16,69	14,07	-27,28	211,80	0,41	5,83
Mud pool	3	SlpD14-TS-L12-01	10	69,569319	-139,016525	403,38	326,89	211,82	4,43	0,29	15,24	0,93	-27,05	211,80	1,54	1,43
Mud pool	3	SlpD14-TS-L13-01	10	69,569781	-139,017766	409,03	320,99	211,82	2,70	0,17	16,01	0,91	-26,60	211,80	1,52	1,38
Mud pool	3	SlpD14-TS-L14-01	10	69,570244	-139,019007	411,42	79,47	211,82	2,03	0,14	14,89	1,40	-26,80	211,80	0,38	0,53
Mud pool	3	SlpD14-TS-N10-01	10	69,567960	-139,015367	398,46	309,11	211,82	2,29	0,13	18,07	1,20	-26,68	211,80	1,46	1,75
Mud Pool	3	SlpD14-TS-N12-01	10	69,568885	-139,017849	403,32	336,56	211,82	1,94	< 0,10	19,41	0,88	-27,07	211,80	1,59	1,40
Mud pool	3	SlpD14-TS-P12-01	10	69,568451	-139,019173	374,73	283,16	211,82	2,67	0,14	19,65	1,22	-27,13	211,80	1,34	1,63
Mud pool	3	SlpD14-TS-P9-01	10	69,567063	-139,015450	412,14	342,88	211,82	2,26	0,12	19,15	1,16	-26,87	211,80	1,62	1,87
Mud Pool	3	SlpD14-TS-R8-01	10	69,566167	-139,015534	450,65	376,06	211,82	2,22	< 0,10	22,21	0,94	-27,02	211,80	1,78	1,68
Mud Pool	3	SlpD14-TS-R9-01	10	69,566630	-139,016775	421,31	347,35	211,82	2,14	< 0,10	21,43	0,85	-27,00	211,80	1,64	1,40
Zone	Zone	Sample_ID	Depth [cm]	Latitude	Longitude	Wet weight	Dry weight	Volume	TC	TN	C/N-ratio	TOC	d13C	Volume (cm3)	BD	SOC (Kg C/m2)
Mud Pool	3	SlpD14-TS-F10-02	30	69,570157	-139,011311	328,81	272,56	211,82	2,61	0,22	11,85	2,10	-26,95	211,80	1,29	8,12
Mud Pool	3	SlpD14-TS-F11-02	30	69,570619	-139,012552	351,67	277,75	211,82	4,20	0,32	13,22	3,47	-27,05	211,80	1,31	13,64
Mud Pool	3	SlpD14-TS-F12-02	30	69,570619	-139,012552	351,94	267,61	211,82	2,87	0,20	14,60	1,72	-26,68	211,80	1,26	6,52
Mud Pool	3	SlpD14-TS-F9-02	30	69,569694	-139,010070	383,34	322,01	211,82	2,30	0,18	12,95	1,65	-26,73	211,80	1,52	7,53
Mud Pool	3	SlpD14-TS-H12-02	30	69,570648	-139,015117	401,65	328,14	211,82	2,15	0,15	14,65	1,34	-26,80	211,80	1,55	6,25
Mud pool	3	SlpD14-TS-L12-02	30	69,569319	-139,016525	409,68	325,78	211,82	2,09	0,14	15,47	1,43	-27,08	211,80	1,54	6,60
Mud pool	3	SlpD14-TS-L13-02	30	69,569781	-139,017766	390,75	301,92	211,82	1,88	0,14	13,64	0,85	-26,40	211,80	1,43	3,62
Mud pool	3	SlpD14-TS-L14-02	30	69,570244	-139,019007	592,49	470,94	211,82	2,47	0,22	10,99	0,67	-26,68	211,80	2,22	4,45
Mud Pool	3	SlpD14-TS-N10-02	30	69,567960	-139,015367	409,80	318,38	211,82	2,30	0,12	18,71	1,05	-26,97	211,80	1,50	4,73
Mud Pool	3	SlpD14-TS-N12-02	30	69,568885	-139,017849	420,90	322,50	211,82	2,35	0,12	19,97	1,03	-26,85	211,80	1,52	4,73
Mud pool	3	SlpD14-TS-P12-02	30	69,568451	-139,019173	359,44	260,59	211,82	2,46	0,12	19,76	0,90	-27,21	211,80	1,23	3,31
Mud Pool	3	SlpD14-TS-P9-02	30	69,567063	-139,015450	416,14	434,20	211,82	2,45	0,11	22,36	1,19	-27,26	211,80	2,05	7,30
Mud Pool	3	SlpD14-TS-R8-02	30	69,566167	-139,015534	422,84	350,10	211,82	2,32	0,11	20,93	0,85	-27,24	211,80	1,65	4,21
Mud Pool	3	SlpD14-TS-R9-02	30	69,566630	-139,016775	431,17	340,48	211,82	2,62	0,13	20,47	1,17	-27,07	211,80	1,61	5,64

Zone	Zone	Sample_ID	Depth [cm]	Latitude	Longitude	Wet weight	Dry weight	Volume	TC	TN	C/N-ratio	TOC	d13C	Volume (cm3)	BD	SOC (Kg C/m2)
Mud Pool	3	SlpD14-TS-F13-01	6	69,571082	-139,013793	275,11	158,99	211,82	4,29	0,31	13,82	3,41	-26,97	211,80	0,75	1,54
Mud Pool	3	SlpD14-TS-H13-01	6	69,571111	-139,016358	392,02	303,65	211,82	2,25	0,16	14,06	1,47	-26,86	211,80	1,43	1,27
Mud pool	3	SlpD14-TS-J14-01	6	69,570677	-139,017683	380,36	289,75	211,82	10,49	0,62	16,97	1,05	-26,82	211,80	1,37	0,86
Zone	Zone	Sample_ID	Depth [cm]	Latitude	Longitude	Wet weight	Dry weight	Volume	TC	TN	C/N-ratio	TOC	d13C	Volume (cm3)	BD	SOC (Kg C/m2)
Mud Pool	3	SlpD14-TS-F10-01	10	69,570157	-139,011311	368,32	306,10	211,82	2,54	0,22	11,31	2,16	-26,66	211,80	1,45	3,12
Mud Pool	3	SlpD14-TS-F11-01	10	69,570619	-139,012552	350,96	266,76	211,82	2,60	0,21	12,17	1,59	-26,73	211,80	1,26	2,00
Mud Pool	3	SlpD14-TS-F12-01	10	69,570619	-139,012552	411,30	332,75	211,82	2,24	0,14	15,56	1,17	-26,78	211,80	1,57	1,84
Mud Pool	3	SlpD14-TS-F9-01	10	69,569694	-139,010070	385,29	320,94	211,82	2,44	0,18	13,48	1,57	-27,02	211,80	1,52	2,38
Mud Pool	3	SlpD14-TS-H12-01	10	69,570648	-139,015117	219,55	87,81	211,82	12,57	0,75	16,69	14,07	-27,28	211,80	0,41	5,83
Mud pool	3	SlpD14-TS-L12-01	10	69,569319	-139,016525	403,38	326,89	211,82	4,43	0,29	15,24	0,93	-27,05	211,80	1,54	1,43
Mud pool	3	SlpD14-TS-L13-01	10	69,569781	-139,017766	409,03	320,99	211,82	2,70	0,17	16,01	0,91	-26,60	211,80	1,52	1,38
Mud pool	3	SlpD14-TS-L14-01	10	69,570244	-139,019007	411,42	79,47	211,82	2,03	0,14	14,89	1,40	-26,80	211,80	0,38	0,53
Mud pool	3	SlpD14-TS-N10-01	10	69,567960	-139,015367	398,46	309,11	211,82	2,29	0,13	18,07	1,20	-26,68	211,80	1,46	1,75
Mud Pool	3	SlpD14-TS-N12-01	10	69,568885	-139,017849	403,32	336,56	211,82	1,94	< 0,10	19,41	0,88	-27,07	211,80	1,59	1,40
Mud pool	3	SlpD14-TS-P12-01	10	69,568451	-139,019173	374,73	283,16	211,82	2,67	0,14	19,65	1,22	-27,13	211,80	1,34	1,63
Mud pool	3	SlpD14-TS-P9-01	10	69,567063	-139,015450	412,14	342,88	211,82	2,26	0,12	19,15	1,16	-26,87	211,80	1,62	1,87
Mud Pool	3	SlpD14-TS-R8-01	10	69,566167	-139,015534	450,65	376,06	211,82	2,22	< 0,10	22,21	0,94	-27,02	211,80	1,78	1,68
Mud Pool	3	SlpD14-TS-R9-01	10	69,566630	-139,016775	421,31	347,35	211,82	2,14	< 0,10	21,43	0,85	-27,00	211,80	1,64	1,40
Zone	Zone	Sample_ID	Depth [cm]	Latitude	Longitude	Wet weight	Dry weight	Volume	TC	TN	C/N-ratio	TOC	d13C	Volume (cm3)	BD	SOC (Kg C/m2)
Mud Pool	3	SlpD14-TS-F10-02	30	69,570157	-139,011311	328,81	272,56	211,82	2,61	0,22	11,85	2,10	-26,95	211,80	1,29	8,12
Mud Pool	3	SlpD14-TS-F11-02	30	69,570619	-139,012552	351,67	277,75	211,82	4,20	0,32	13,22	3,47	-27,05	211,80	1,31	13,64
Mud Pool	3	SlpD14-TS-F12-02	30	69,570619	-139,012552	351,94	267,61	211,82	2,87	0,20	14,60	1,72	-26,68	211,80	1,26	6,52
Mud Pool	3	SlpD14-TS-F9-02	30	69,569694	-139,010070	383,34	322,01	211,82	2,30	0,18	12,95	1,65	-26,73	211,80	1,52	7,53
Mud Pool	3	SlpD14-TS-H12-02	30	69,570648	-139,015117	401,65	328,14	211,82	2,15	0,15	14,65	1,34	-26,80	211,80	1,55	6,25
Mud pool	3	SlpD14-TS-L12-02	30	69,569319	-139,016525	409,68	325,78	211,82	2,09	0,14	15,47	1,43	-27,08	211,80	1,54	6,60
Mud pool	3	SlpD14-TS-L13-02	30	69,569781	-139,017766	390,75	301,92	211,82	1,88	0,14	13,64	0,85	-26,40	211,80	1,43	3,62
Mud pool	3	SlpD14-TS-L14-02	30	69,570244	-139,019007	592,49	470,94	211,82	2,47	0,22	10,99	0,67	-26,68	211,80	2,22	4,45
Mud Pool	3	SlpD14-TS-N10-02	30	69,567960	-139,015367	409,80	318,38	211,82	2,30	0,12	18,71	1,05	-26,97	211,80	1,50	4,73
Mud Pool	3	SlpD14-TS-N12-02	30	69,568885	-139,017849	420,90	322,50	211,82	2,35	0,12	19,97	1,03	-26,85	211,80	1,52	4,73
Mud pool	3	SlpD14-TS-P12-02	30	69,568451	-139,019173	359,44	260,59	211,82	2,46	0,12	19,76	0,90	-27,21	211,80	1,23	3,31
Mud Pool	3	SlpD14-TS-P9-02	30	69,567063	-139,015450	416,14	434,20	211,82	2,45	0,11	22,36	1,19	-27,26	211,80	2,05	7,30
Mud Pool	3	SlpD14-TS-R8-02	30	69,566167	-139,015534	422,84	350,10	211,82	2,32	0,11	20,93	0,85	-27,24	211,80	1,65	4,21
Mud Pool	3	SlpD14-TS-R9-02	30	69,566630	-139,016775	431,17	340,48	211,82	2,62	0,13	20,47	1,17	-27,07	211,80	1,61	5,64

$$SOC[KgC/m^2] = \frac{bulkdensity \cdot TOC[\%] \cdot depth[cm]}{10}$$

Danksagung

Zuerst möchte ich mich bei Prof. Dr. Lantuit und George Tanski bedanken, die es mir ermöglicht haben, meine Arbeit am Alfred-Wegener-Institut in Potsdam zu schreiben. Beide haben mir eine optimale Betreuung geboten und standen mir jeder Zeit für Fragen zur Verfügung. Herzlichen Dank auch an Dr. Michael Fritz, für die Begutachtung dieser Arbeit.

Vielen Dank an Birgit Plessen und Sylvia Pinkerneil f ür die Messungen von $\delta^{13}C_{org}$ am GFZ! Weiter möchte ich Dyke Scheidemann und Daniel Gorzawski für die Einarbeitung und Betreuung im Labor danken. Vielen Dank auch an das COPER-Team, die mich sofort sehr freundlich aufgenommen haben, sodass ich immer gerne am AWI gearbeitet habe und mich dort immer sehr wohl gefühlt habe. Für das Aufmuntern und die unterhaltsamen Pausen am AWI möchte ich speziell Isabell danken!

Besonderen Dank an meinen Bruder Sven, der mir das Programm LaTeX näher gebracht hat und mir rund um die Uhr für Fragen zur Verfügung stand! Danke Sveni!!! Großen Dank gilt meinen Eltern, Ingrid und Christian, für die finanzielle Unterstützung und vor allem den Glauben in mich, dass zu schaffen, was ich mir vornehme und den Mut nicht zu verlieren.

Selbstständigkeitserklärung

Ich versichere hiermit,

1. dass ich die vorliegende Arbeit selbständig und ohne unerlaubte Hilfe angefertigt habe.
2. dass ich keine anderen als die angegebenen Quellen, die Übernahme wörtlicher Zitate aus der Literatur, sowie die Verwendung der Gedanken anderer Autoren an den entsprechenden Stellen innerhalb der Arbeit gekennzeichnet habe.
3. dass alle Abbildungen und Fotos, wenn nicht anderweitig gekennzeichnet, vom Autor selbst erstellt wurden.
4. dass diese Arbeit bisher in dieser oder ähnlicher Form bei keiner Fakultät, weder dieser noch einer anderen Hochschule, eingereicht wurde.

Potsdam, 14.12.2015

_____

Unterschrift (Saskia Ruttor)